CHAPTER III

XENOLITHS

3.1 Introduction

The basaltic flows exposed in the areas of Nguu Hills, located NE of Simba, and Ngulai Hills, located NE of Emali, bear abundant xenoliths which vary in compositions from ultramafic to mafic compositions, including ruby-bearing ones. The deep-seated xenoliths can be subdivided into 3 groups based upon their physical appearances: (1) peridotites, (2) pyroxenites, and (3) granulites. Peridotite xenoliths are sparingly found as small nodules, in a scale of only few centimeters, disseminated in the basalts, and barely observed as loose xenoliths on the ground. These xenoliths exhibit a granular texture resembling those found elsewhere. Pyroxenite xenoliths, generally with obvious polygonal texture on weathered surfaces, are found in subordinate amount and comparatively larger in size, but rarely over 10 cm across. Granulites are the most abundant xenoliths observed and the majority of this group is mafic in composition. This group, with a maximum size bigger than 25 cm across, shows various appearances such as non-foliated, foliated, and composite banded between light and dark colors. The light layers are dominated by plagioclase and kelyphitic reaction rinds. The dark layers are dominated by pyroxene. The observed thickness of these bands varies from sample to sample, in a scale of few millimeters to more than 6 cm. Despite of being found as sub-rounded massive nodules, the overall appearances of the pyroxenites seem identical to those of the dark bands of the mafic granulites. In addition, some xenolithic fragments of the underlain Precambrian basement complexes of Kasigau Series, including amphibolites, gneisses and felsic granulites, are also common. These crustal xenoliths, however, are not emphasized in this study.

Comparatively, the xenoliths observed in the vicinity of Nguu Hills are more or less akin to those found in the Ngulai Hills area in all physical aspects, varieties and size ranges. Nevertheless, the peridotites are rarely found in the later locality. The pyroxenites, on the other hand, are more abundant and have coarser grain sizes, particularly around Kwanthuku hill where floats of clinopyroxene megacrysts are also common.

3.2 Petrographic Description

Total 50 xenolith specimens were selected for petrographic investigation. They include 2 peridotite samples, 12 pyroxenite samples, and 36 granulite samples. Lithology and mineral assemblage of these specimens are summarized in Table 3.1. Modal analyses of the selected peridotite and pyroxenite xenoliths, using an application of EPMA, qualitative multi-elemental mapping, are presented in Figure 3.1. Detailed petrographic descriptions of these xenolith groups are reported below.

3.2.1 *Group 1: Peridotites*

There are two specimens, *Ng07* and *Ng18* (Figure 3.2*a*), of this group which are suitable for both petrographic and geochemical observations. Modal classification of these xenoliths, estimated using EPMA multi-element scanning technique, is presented in Figure 3.1. They are respectively classified as spinel lherzolite and spinel wehrlite. They mainly contain olivine (40-48%) and clinopyroxene (37-42%). Orthopyroxene is subordinately observed (2-20%). Anhedral spinel (3-5%) is an essential interstitial mineral occurred.

3.2.1.1 Spinel lherzolite xenolith (*Ng07*) displays a fine-grained inequigranular (≤1-2mm) cumulus texture (Figure 3.2*b*). Triple-junction contacts among olivine, orthopyroxene and clinopyroxene grains are common. Sieve texture overprinted on some large orthopyroxene can be observed, but not exsolution lamella. There are two color varieties of spinel, e.g. pale greenish brownish yellow (0.7-1.6mm) and reddish brown (0.05-0.5mm), coexisted. Some large spinels contain pyroxene inclusions. Local kelyphitization is observed along grain boundaries, cracks, or pervasively develops into web-liked network of polygonal kelyphitic garnets invading into large primary olivine and orthopyroxene grains. Where a cluster of polygonal kelyphites come in contact with spinel, a thin symplectic corona containing plagioclase between them (Figure 3.3*d*) is always seen. Radial cracks are always associated with these polygonal kelyphitic garnet clusters. Second generation of finer polygonal outlined orthopyroxene and clinopyroxene is developed in association with polygonal kelyphictic garnet clusters.

.3.1.2 Spinel wehrlite xenolith (*Ng18*) has faint alignment of olivine and pyroxene grains observable on rough specimen surfaces and macroscopically exhibits

Table 3.1 Types of xenoliths from the study area. Numbers begun with *Ng* are from the Nguu Hills and the others from the Ngulai Hills. New forming mineral phases are in brackets.

Note: Specimens in bold italic numeric were selected for XRF, underlined ones for ICPMS, and asterisk marked (*) for EPMA.

Group	Lithology	Mineral Assemblage	Specimen
Peridotite	Spl lherzolite	Ol + Cpx +Opx + Spl +Ilm +Grt(Kely)+(Pl)	Ng***07****
	Spl wehrlite	Ol + Cpx + Opx + Spl + (Kely)	Ng***18****
Pyroxenite	*Plagioclase-free*		
	• Orthopyroxenite	Opx + Cpx+(Kely)	Ng33*, KNt***03****
	• Websterite	Opx + Cpx +(Kely) (±Qtz)	Ng***12****, ***22***, ***29***, ***34****
	Plagioclase-bearing		
	• Spl websterite	Cpx + Opx + Spl± Pl relict (Kely, ± Qtz, ± Ky)	Ng***24***, ***25****, ***27****
	• Crn-spl websterite	Cpx + Opx + Spl + Crn +Pl relict (Kely, ± Qtz, ± Ky)	Ng***02***, ***10***, ***23****, ***36***
Granulite	*Crn-bearing mafic granulite*		
	• Composite banded	Pl + Cpx + Opx + Crn ± Spl (Kely ± Grt, +Ky, ± Qtz)	Ng***05***, ***06***, ***13****, ***14****, ***15***, Ng***17***, ***20***, ***21****, ***26***, 28*, Ng***30****, ***32***, KKa01, ***03***, KNt***02****, OK01
	• Foliated	Pl + Cpx + Opx + Crn ± Spl (Kely± Grt, + Ky, ± Rt ± Qtz)	Ng***03***, ***04***, ***09***, ***11***, 14-2, 16, ***19***, ***31***, 35, ***38***, 39, ***40***, KKa02, ***04****, KNt01*, Kyd01, OK***02****, ***03****
	Crn-barren granulite (non-foliated)		
	• Felsic composition	Pl + Cpx + Opx (Kely, + Ky, ± Qtz)	KMb***01****
	• Mafic composition	Cpx + Pl + Opx (Kely, + Ky, ± Qtz)	Ng***37****

Mineral abbreviations are after Kretz (1983): Ol – olivine; Cpx – clinopyroxene; Opx – orthopyroxene; Spl – spinel; Ilm – ilmenite; Rt- rutile; Crn – corundum; Pl – plagioclase; Ky – kyanite; Grt – garnet; Qtz – quartz; Kely – kelyphite

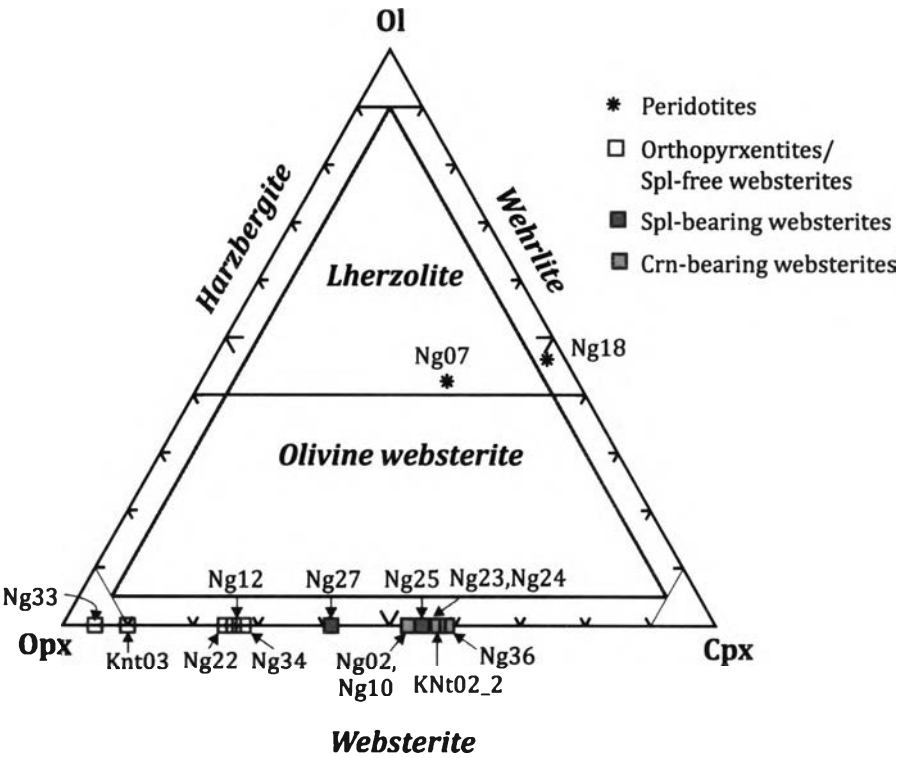

Figure 3.1 Modal proportions for olivine (Ol), orthopyroxene (Opx) and clinopyroxene (Cpx) of peridotite xenoliths and pyroxenite xenoliths from the study areas. Filled square represents corundum-bearing variety.

a fine-grained (1-2 mm) equigranular cumulus texture. Corona textures around pyroxene and spinel are common. Thin kelyphite-plagioclase symplectic coronas around pyroxene as well as secondary spinel-orthopyroxene-sapphirine(?) symplectite around spinel are locally observed. Kelyphitization affects the entire rock, but occurs in less pervasive fashion and mostly forms around clinopyroxene and spinel grains. However, remained relic garnets in side kelyphites are not observed. At the center of all the clinopyroxenes, a cloud of black tiny spots is usually observed and left the outer part of the grain as an unaffected ring.

Along with a later developed metamorphic polygonal mosaic texture, both specimens still preserve their original igneous texture in part. Triple-junctions among the primary phases suggest that these rocks have attained an equilibrium stage. The polygonal kelyphitic garnet networks around spinel in sample *Ng07*, nevertheless, suggest this spinel lherzolite was undergone a transformation process of spinel-garnet stability field. However, the reaction corona between spinel and garnet may indicate instability between spinel and relic garnet during a relatively late evolution

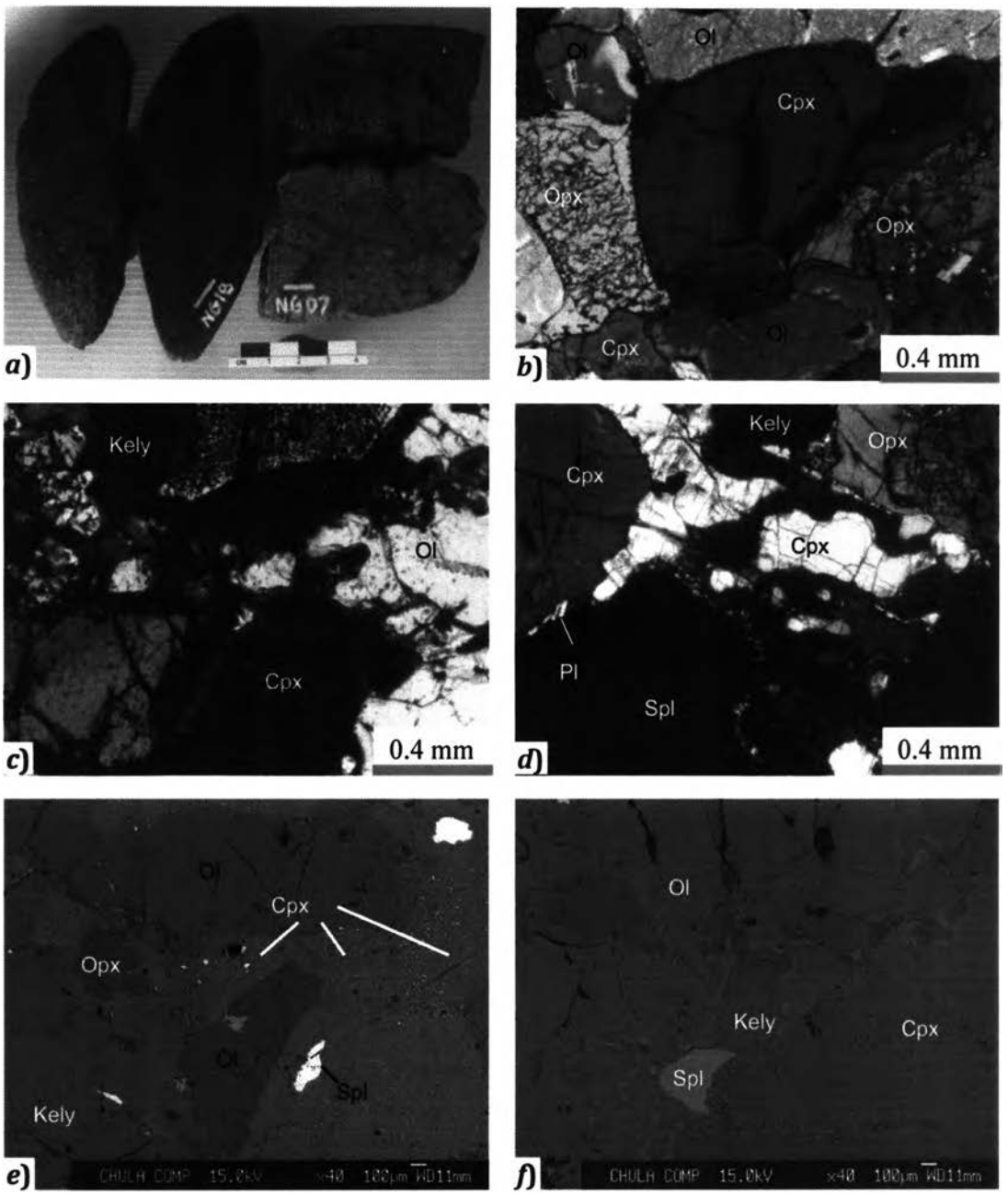

Figure 3.2 **Group 1 xenoliths selected for petrographic study: *a*) Spl wehrlite (*Ng18*: left) and Grt-Spl lherzolite (*Ng07*: right). *b*) (*Ng07*) Opx is in mutual contact with Ol and Cpx (*Ng07*). *c*) (*Ng 18*) Mottled clinopyroxenes (Cpx), with spongy textures and kelyphite rims, are in mutual contact with unaltered olivine (Ol). *d*) (*Ng07*) Thin reaction zone containing small plagioclase grain at a spinel (spl) rim. *e)* (*Ng18*) Back-scattered electron (BSE) image reveals fine exsolution lamella (at the lower right corner) and mottled texture in Cpx as well as reaction rind around Spl. *f*) (*Ng07*) BSE image shows spongy texture on a part of Cpx and Spl encrusted by patches of kelyphite taking spaces between Ol and Cpx.**

stage of the rock, probably involved by hot basaltic magma during transportation onto the surface. The sieve texture on orthopyroxene grain confirms that these xenoliths subsequently experienced a decompression cooling event. In addition, an event of weak metasomatic overprint on the xenoliths can be denoted by the presence of brown fibrous-like kelyphite as well as a cloud of black spots inside clinopyroxene as observed in Ng18.

3.2.2 *Group 2: Pyroxenites*

The common features of the xenoliths of this group are pyroxene rich, lack of olivine and less observable plagioclase in hand specimens (Figure 3.3). Based on mineral modal in conjunction with the presence of corundum grains in hand specimen, the pyroxenites can be differentiated into 4 varieties (Table 3.1) including orthopyroxenite, websterite, spinel websterite and corundum-spinel websterite. Out of those 12 pyroxenite specimens, four contain visible minute grains of pink corundum (ruby).

3.2.2.1 Orthopyroxenite xenoliths (*KNt03* and *Ng33*) bear a minor amount of cpx (5-10%) and are medium- to coarse-grained (2-8mm.). They are dark brownish black in color and exhibit an equigranular granoblastic texture with polygonal grain outlines on both macroscopic and microscopic views, and are not distinguishable macroscopically from some of websterite xenoliths, e.g. *Ng22* (Figure 3.3a). Thin kelyphite network around pyroxenes and exsolution lamella in orthopyroxenes are common features (Figure 3.3f). Clinopyroxenes occur as small interstitial grains and are prone to be overprinted by a cloud of black spots.

3.2.2.2 Websterite xenoliths (*Ng12, 22, 29* and *34*) are composed mainly of orthopyroxene, with a subordinate amount of clinopyroxene (25-28%) and kalyphite (10-15%). Clinopyroxenes are medium-grained (1-3 mm.), with a dark brownish black color, and exhibit an equigranular granoblastic texture, with distinctive polygonal grains (Figures 3.3a and b). Due to their similar appearances, the websterites can be distinguished from the orthopyroxenites only by microscopic investigation. Along grain boundaries, orthopyroxenes are commonly replaced by double reaction coronas of second generation clinopyroxene and kelyphitic garnet chains (Figure 3.3c). The garnet grains, with better developed polygonal outlines compared to those observed in orthopyroxenites, are totally kelyphitized. Rare

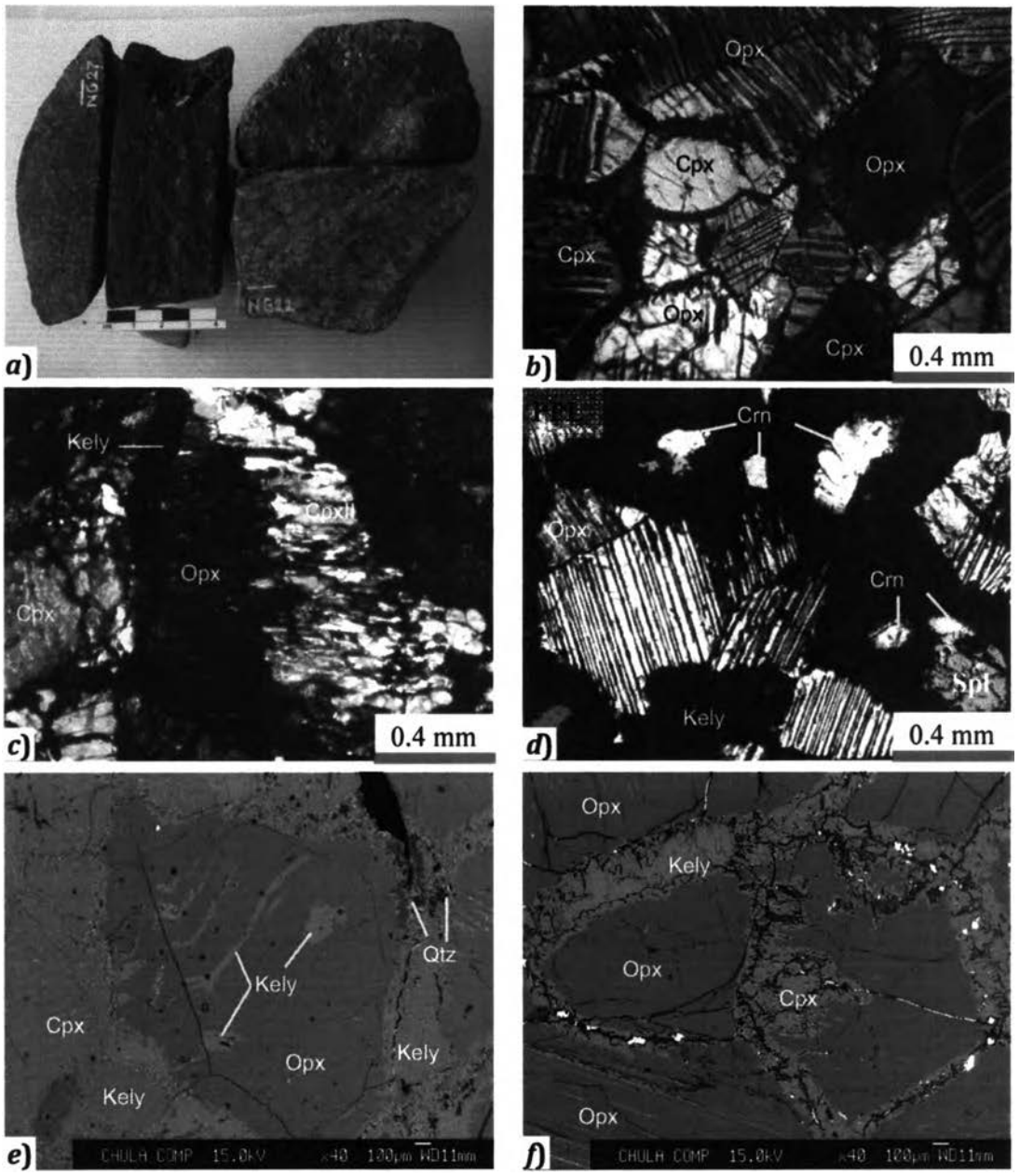

Figure 3.3 **Group 2 pyroxenite xenoliths selected for petrographic study: a) Medium-grained websterite (*Ng22*) and fine-grained spinel websterite (*Ng27*). *b*) (*Ng12*) Granoblastic texture of Opx and Cpx with exsolution lamella and rimmed by thin kelyphictic garnet network. *c*) (*Ng22*) Opx is overgrown by 2nd clinopyroxene (CpxII). *d*) (*Ng 23*) kelyphite (Kely) corona cored with corundum (Crn) and green spinel (Spl). Crn in contact with spl is observed in Crn-bearing websterite. e) (*Ng12*) Back-scattered electron (BSE) image of the websterite showing kelyphite infilled along bended cleavages of Opx. Small quartz (Qtz) grains occur within reaction band rimming Opx. *f*) (*Ng33*) BSE image of the orthopyroxenite showing kelyphitic corona around Opx that is partly turned to Cpx.**

quartz grains are formed as tiny strings (≤0.8 mm long) located at the edge of pyroxene in contact with kelyphite network (Figure 3.3e). Regardless the absence of olivine and spinel, and more pronounced exsolution lamellae, both the orthopyroxenites and websterites are very akin to the spinel wehrlite in terms of overall microscopic appearances.

3.2.2.3 Spinel websterite xenoliths (*Ng24, 25* and *27*) can be discriminated from the aforementioned varieties by their color of medium bluish gray and lack of clear polygonal outlines due to the intense reaction rind along pyroxene grain boundaries observable under a loupe. They are medium-grained (1-3 mm) with equigranular granoblastic texture. They are composed of roughly equal amounts of orthopyroxene and clinopyroxene (35-40% each), garnet and spinel. Spinel, with pale greenish brown yellow color, is mantled by a kelyphitic network. Plagioclase is another accessory phase found in some specimen. The plagioclase, where present, barely preserves its original texture and always breaks down into very fine-grained mass, and may contain several minute rods of kyanite, identified via RAMAN peak pattern, generally in a size of smaller than 50 microns. The kyanite seems to align along cleavage traces of original plagioclase. These kyanite inclusions appear stable inside the host and no evidence of inversion to sillimanite is observed. Quartz may be developed as a reaction phase associated with pyroxene either along cleavage traces or along the edges of the grains, which are in contact with garnet coronas.

3.2.2.4 Corundum-spinel websterite xenoliths (*Ng02, 10, 23* and *36*) are medium-grained (1-3 mm) with a granoblastic texture, and composed of orthopyroxene, clinopyroxene, plagioclase, spinel, kelyphite, kyanite and minor quartz. These xenoliths are almost indifferent from the spinel websterites, except slightly lighter in color, having tiny ruby (<1 mm in length) scattered in the matrix, and more abundance of plagioclase.

The original igneous textures of these pyroxenite xenoliths in every specimen investigated are mostly overprinted either by a metamorphic polygonal mosaic texture or a corona texture. Spinel and corundum are always encapsulated by kelyphite corana and never found in mutual contact with pyroxene. These all indicate that the pyroxenite xenoliths were experienced a metamorphic overprint beyond their original equilibrium stage.

3.2.3 *Group 3: Granulites*

Based on the presence or absence of minute pink corundum grains (mostly <1 mm in length) in hand specimens, the xenoliths of this group are divided into 2 subgroups, e.g. (1) corundum-bearing granulite and (2) corundum-barren granulite. The later type is comparatively rare and only 2 specimens were obtained for investigation. The modal mineral compositions of these mafic granulite xenoliths vary from one specimen to another. However, plagioclase content is always greater than 20% by mode.

3.2.3.1 Corundum-bearing mafic granulite xenoliths consists of plagioclase (20-40%), clinopyroxene (20-40%), orthopyroxene (up to 30%), kelyphitic garnet (30-60%), pink corundum (up to 5%) and kyanite. Quartz, spinel and rare rutile may be present in the xenoliths. Several specimens exhibit distinctive composite layering between dark-colored pyroxene-rich and light-colored plagioclase-rich bands (Figure 3.4a). Some samples may not show such distinctive banding but a foliated feature due to plastic deformation is obvious (Figure 3.4b). All the mafic granulitic xenoliths display conspicuous reaction corona textures, particularly in a plagioclase-dominated zone, caused by the interaction between coarse primary orthopyroxene and plagioclase. Kelyphite observed along exsolution lamella of pyroxene is not uncommon. Relict garnet may be observed as a core of kelyphitic grains in some specimens (Figure 3.4d), e.g. *KKa01*, *KKa04*, *KNt01* and *KNt02*. Plagioclase is totally recrystallized into small grains but its original relict still preserved. Within the plagioclase relict, abundant tiny needles inclusions of Al-silicate (few tens of microns in size) are aligned along the directions of plagioclase cleavage. Raman analyses indicate that these needles are kyanite. Orthopyroxene and corundum as well as greenish spinel are always mantled by kelyphitic coronas. Complex coronas around the relict orthopyroxene grains have the inner zone comprising medium-grained granular clinopyroxene or intergrowths of clinopyroxene and quartz rimmed by plagioclase. The outer zone contains kelyphitic garnet with euhedral crystal faces towards the matrix plagioclase grains. A sieve or a spongy texture overprinted on pyroxene is common. Direct contact between corundum and spinel is rarely observed (only in *KNt02*). Mutual contact between corundum and plagioclase, however, is present in few specimens, e.g. KNt01 and 02. Rutile occurs as anhedral tiny grains, barely larger than 50 μm across (*KNt02*), disseminated

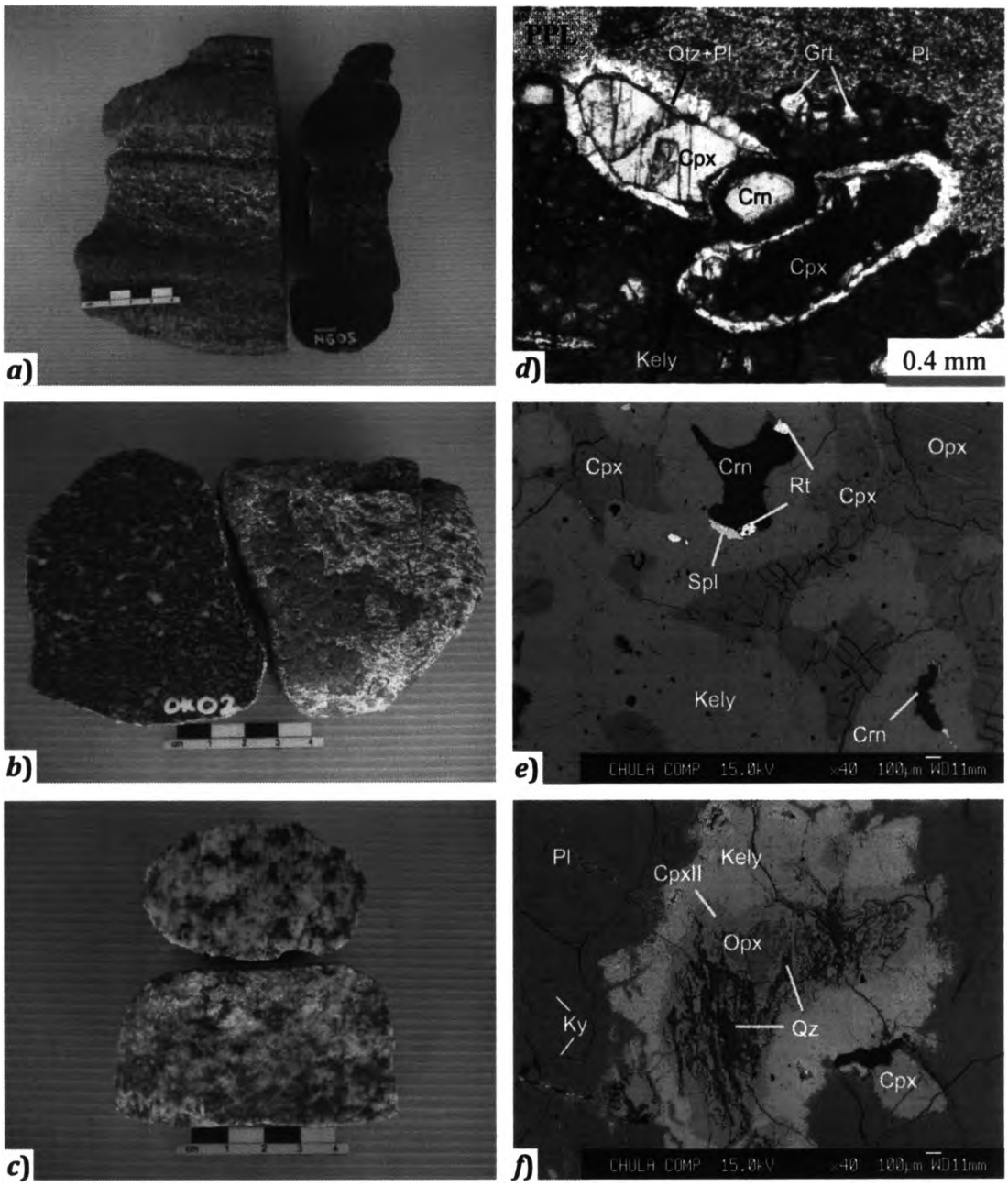

Figure 3.4 **(Left) Major varieties of rough specimens of group 3 mafic granulite xenoliths: *a*) Sharp banded corundum (Crn)-bearing (Ng27), *b*) Foliated Crn-bearing (OK02), and *c*). non-foliated, polygonal Crn-barren (KMb01). (Right) Photo images: *d*) (KKa04) showing cluster of polygonal kelyphite (Kely) with garnet (Grt) cored in contact with clinopyroxene (Cpx), Crn and recrystallized plagioclase (Pl). Thin corona of quartz (Qtz) wrapping Cpx is expressed. *e)* (KNt02) Back-scattered electron (BSE) image displaying Crn in direct contact with Spl and rutile (Rt). *f*). (KMb01) BSE image showing orthopyroxene (Opx), with strings of Qtz intergrowth, mantled by CpxII and kelyphitic coronas, and Pl with needle-shaped kyanite (Ky) inclusions.**

in pyroxene grains and as an interstitial phase, and is occasionally found in direct contact at the edges of corundum grains (Figure 3.4e). Anhedral quartz strings formed either along cleavage traces or in the reaction rim zone of orthopyroxene can be seen in several specimens, e.g. *Ng13*, *Ng39*, *KKa01*, *KNt01*, *KNt02* and *OK01*.

3.2.3.2 Corundum-barren granulite xenoliths are composed of two compositional varieties; one has felsic composition with anorthositic appearance (*KMb01*, Figure 3.4c) and the other has a mafic composition (*Ng37*) similar to the corundum-bearing type. The anorthositic xenolith is composed mainly of plagioclase (up to 85%) and kelyphite (10-30%). Clinopyroxene and orthopyroxene (<10%) are present as a minor phases. The orthopyroxene mostly remains as clinopyroxene cores. Polygonal of relatively equigranular granoblastic assemblages are very pronounced on hand-specimen surfaces. Microscopically, double reaction aureoles of kelyphite and clinopyroxene around orthopyroxene core are locally common. Plagioclase still retains its polygonal outline but displays wavy extinction. It is much less affected by a recrystallization process. Inside the plagioclase, abundant tiny kyanite needle inclusions, as seen in the corundum-bearing mafic granulite, are always present (Figure 3.4f). Quartz formed as strings along cleavage traces of orthopyroxene are commonly observed (Figure 3.4f).

Very similar corona complex mantling pyroxene as observed here were also reported from meta-igneous granulite xenoliths of eastern Autralia (e.g. Griffin *et al.*, 1990) and of nearby Chyulu Hills. (Henjes-Kunst and Altherr, 1992). A foliation texture together with wavy extinction of plagioclase indicates that all the granulitic xenoliths have somehow experienced stress condition in different degrees. The corundum-bearing granulites are prone to undergo garnetization compared to the corundum-barren granulite. The decomposed textures of pyroxenes could either represent a rapid decompression cooling or the result of the interaction between the hosted xenoliths and the magma in the latest event prior to surface exposure. Texturally, the compositional banding and other features observed suggest that the xenoliths were firstly formed through a magmatic segregation, rather than solely created through metamorphic processes, and later partly overprinted by plastic deformation texture and reaction textures.

The common textural association between kyanite rods and plagioclase hosts, in the spinel (±corundum) websterite and all granulite samples, has also been

observed in garnet-scapolite-kyanite granulite xenoliths from Neogene Lashaine volcano in northern Tanzania as investigated by Jones *et al.* (1983). This texture indicates crystallization of kyanite during deformation of the plagioclase, most likely by an exsolution process from plagioclase, of which the anorthite component was converted into the grossular component of garnet, kyanite and quartz as the following equation (Goldsmith, 1980):

$$3CaAl_2Si_2O_8 \longrightarrow Ca_3Al_2Si_3O_{12} + Al_2SiO_5 + SiO_2$$

According to Holdaway (1971), Jones *et al.* (1983) estimated the stability condition for their kyanite-bearing xenoliths in a temperature range of about 1,200°K (~927°C) with a minimum pressure of ~13 kb.

3.2 Geochemistry of Xenoliths

Forty xenoliths were selected for major oxide analyses and 25 out of 40 were analyzed for trace elements concentrations. Whole-rock major oxides and CIPW normative compositions of representative samples are presented in Table 3.2. Selected trace element analyses are given in Table 3.3.

According to chemical classification schemes, such as the total alkali vs SiO_2 plot of LeBas *et al.* (1982) and R1-R2 diagram of De la Rhoce (1980), the studied xenoliths are chemically equivalent to basaltic compositions, ranging from picrobasalt to basalt (Figure 3.5a) and belong to subalkaline affinity (Figure 3b). These diagrams clearly show chemical separation between the xenoliths and the host basalts. The granulite xenoliths seem to develop a broad defined trend, upon total alkaline variation observed, parallel to those of the basats. Based on the CIPW norm calculation, they have a high narrow Mg# values ranging from about 0.73 to 0.84 and are indifferent among groups of the xenoliths. Their An contents are in a wider range from approximately 61 to 94.

In terms of major oxides contents, the peridotite samples, *Ng07* and *Ng 18*, have SiO_2 between 40.3 and 43.1 wt %, MgO around 30 wt %, $Fe_2O_3^t$ from 14.6 to 17.5 wt % and Al_2O_3 from 5.8 to 7.7 wt %, with highest An values of around 94 and relatively high Mg# values are from 0.78 to 0.82. The sample Ng 07 also have corundum normative, which is rather unusual compared to normal peridotite The abundance of Cr is remarkably high for this group varying from ~2,800 to 4,000

Table 3.2 Whole-rock major oxide analyses and CIPW normative mineralogy of representative samples of each specimen group of xenoliths, analyzed by WD-XRF.

	Peridotites		Pyroxenites					
	Spl lherzolite	Spl wehrlite	Webs.	Webs.	Px-rich band*	Spl webs.	Spl webs.	Spl-Crn webs.
wt %	NG 07	NG 18	NG 12	NG 29	KNt 02-2*	NG 27	NG 25	NG 23
SiO_2	40.29	43.05	50.64	49.20	48.63	44.26	49.63	46.79
TiO_2	0.08	0.51	0.25	0.38	0.74	0.08	0.34	0.16
Al_2O_3	7.71	5.76	7.90	7.52	9.02	17.37	13.21	16.98
[1]Fe_2O_3	1.79	2.89	1.24	2.68	10.44	5.05	2.33	3.28
[2]FeO	14.09	10.58	8.52	10.05	1.47	5.20	6.36	6.28
MnO	0.20	0.19	0.18	0.23	0.19	0.14	0.17	0.16
MgO	30.43	29.86	24.44	20.08	18.44	18.14	14.87	14.67
CaO	3.40	5.39	5.17	7.76	9.66	8.07	10.59	9.51
Na_2O	0.12	0.15	0.34	0.64	0.55	0.80	1.03	1.15
K_2O	n.d.	n.d.	0.01	n.d.	n.d.	n.d.	n.d.	n.d.
P_2O_5	n.d.	0.06	0.01	n.d.	0.05	n.d.	n.d.	n.d.
$H2O^+$	n.d**	n.d**	0.06	0.01	0.26	n.d**	0.38	n.d**
H_2O^-	0.21	0.27	0.13	0.21	0.27	0.21	0.26	0.21
Total	*100.14*	*100.12*	*99.71*	*99.67*	*99.61*	*99.68*	*99.61*	*99.77*
wt %	**CIPW normative mineralogy (%)[3]**							
Quartz	0.00	0.00	0.00	0.00	2.88	0.00	0.00	0.00
Orthoclase	0.00	0.00	0.06	0.00	0.00	0.00	0.00	0.00
Albite	1.02	1.27	2.88	5.42	4.65	6.77	8.72	9.73
Anorthite	16.87	15.05	20	17.65	22.14	40.04	31.42	41.17
Corundum	1.33	0.00	0.00	0.00	0.00	1.38	0.00	0.00
Diopside	0.00	8.99	4.44	16.69	19.81	0.00	16.83	4.78
Hypersthene	14.26	20.95	58.33	44.29	36.74	25.87	35.06	26.02
Olivine	61.89	46.9	10.69	9.89	0.00	17.58	2.48	12.22
Magnetite	2.60	4.19	1.80	3.89	3.21	7.32	3.38	4.76
Ilmenite	0.15	0.97	0.47	0.72	1.41	0.15	0.65	0.30
Hematite	0.00	0.00	0.00	0.00	8.22	0.00	0.00	0.00
Apatite	0.00	0.14	0.02	0.00	0.12	0.00	0.00	0.00
[4]*AN*	*94.32*	*92.44*	*87.42*	*76.52*	*82.63*	*85.54*	*78.29*	*80.88*
[5]*Mg#*	*0.78*	*0.82*	*0.83*	*0.76*	*0.84*	*0.81*	*0.78*	*0.77*

*Pyroxenite-dominated band taken from a corundum-bearing granulite, KNt02, of which the band is thick enough to be separated out for analysis and modally equivalent to websterite.

n.d. = not detected; n.d.** = not determined due to a weight-gaining effect caused by an oxidation of Fe^{2+} to Fe^{3+}.

[1]Fe_2O_3 is derived from $Fe_2O_3^{(total)}$ from XRF method subtracted by FeO from a titration technique.

[2]FeO is obtained from wet chemical analyses.

[3]Calculated using software IgPet2007.

[4]*AN* is an An content in plagioclase calculated using atomic proportion = Ca/ (Ca+2Na).

[5]*Mg#* is calculated using atomic proportion = Mg/(Mg+Fe^{2+}).

Table 3.2 (cont.)

	Granulites							
	Banded	Banded	Banded	Pl-rich band*	Foliated	Foliated	Foliated	Crn-barren
wt %	NG 13	NG 20	KKa03	KNt 02-1*	OK 02	NG 04	OK 03	KMb 01
SiO_2	44.41	46.99	48.68	45.70	49.73	48.84	50.27	51.79
TiO_2	0.10	0.13	n.d.	0.08	0.03	0.11	0.07	0.03
Al_2O_3	17.53	19.41	23.34	27.36	21.64	24.62	24.34	27.65
[1]Fe_2O_3	2.40	2.79	1.83	1.38	1.79	1.59	1.61	0.69
[2]FeO	7.07	5.38	3.50	4.93	3.50	3.05	2.68	0.63
MnO	0.14	0.13	0.07	0.07	0.09	0.06	0.06	0.02
MgO	17.60	12.25	8.60	8.48	7.99	6.67	5.73	1.88
CaO	8.73	10.11	9.51	8.14	10.35	10.02	10.10	11.42
Na_2O	0.87	1.53	2.42	2.57	3.33	3.33	3.43	3.87
K_2O	0.02	0.05	0.15	0.11	0.12	0.14	0.19	0.31
P_2O_5	n.d.	n.d.	n.d.	n.d.	n.d.	n.d.	n.d.	n.d.
$H2O^+$	0.05	0.30	0.99	0.30	0.67	0.83	0.80	1.16
H_2O^-	0.14	0.25	0.40	0.25	0.29	0.30	0.31	0.34
Total	*99.70*	*99.66*	*99.49*	99.66	*99.62*	*99.60*	*99.57*	*99.51*
wt %	CIPW normative mineralogy (%)[3]							
Qtz	0.00	0.00	0.00	0.00	0.00	0.00	0.00	0.56
Or	0.12	0.30	0.89	0.65	0.71	0.83	1.12	1.83
Ab	7.36	12.95	20.48	21.75	28.18	28.18	29.02	32.75
An	43.31	45.95	47.18	40.38	43.74	49.71	50.11	56.65
Crn	0.20	0.00	1.91	8.21	0.00	0.77	0.13	0.18
Di	0.00	3.35	0.00	0.00	6.06	0.00	0.00	0.00
Hy	17.29	20.45	21.33	17.04	5.04	5.38	10.05	5.26
Ol	26.92	11.48	3.66	8.64	12.19	11.05	5.59	0.00
Mt	3.48	4.05	2.65	2.00	2.60	2.31	2.33	1.00
Il	0.19	0.25	0.00	0.15	0.06	0.21	0.13	0.06
Hem	0.00	0.00	0.00	0.00	0.00	0.00	0.00	0.00
Ap	0.00	0.00	0.00	0.00	0.00	0.00	0.00	0.00
[4]*AN*	*85.47*	*78.02*	*69.73*	*65.00*	*60.82*	*63.82*	*63.32*	*63.37*
[5]*Mg#*	*0.79*	*0.77*	*0.78*	*0.73*	*0.77*	*0.76*	*0.75*	*0.78*

*Separated plagioclase-dominated band taken from a corundum-bearing granulite, KNt02.
n.d. = not detected.
[1]Fe_2O_3 is derived from $Fe_2O_3^{(total)}$ from XRF method subtracted by FeO from a titration technique.
[2]FeO is obtained from wet chemical analyses.
[3]Calculated using software IgPet2007.
[4]*AN* is an An content in plagioclase calculated using atomic proportion = Ca/ (Ca+2Na).
[5]*Mg#* is calculated using atomic proportion = Mg/(Mg+Fe^{2+}).

Table 3.3 Whole-rock trace element analyses of representative samples of each specimen group of xenoliths, analyzed by ICP-MS.

	Peridotite		Pyroxenite					
	Spl lherzolite	Spl wehrlite	Webs.	Webs.	Px-rich band*	Spl webs.	Spl webs.	Spl-Crn webs.
ppm:	*NG 07*	*NG 18*	*NG 12*	*NG 29*	*KNt 02-2**	*NG 27*	*NG 25*	*NG 23*
Rb	0.60	0.23	0.18	1.56	0.53	0.45	0.53	0.22
Ba	370	13	10	20	71	17	168	58
Sr	48	34	28	61	43	92	142	89
V	45	138	174	301	299	38	232	92
Cr	2801	3984	4464	857	1822	136	916	332
Ni	1414	1614	661	582	842	779	436	493
Zr	1.74	9.29	7.16	4.31	22.56	0.44	3.98	2.44
Sc	2	18	29	33	8	7	36	17
Cu	2	98	65	3	166	2	4	2
Nb	0.41	0.18	0.27	0.23	0.29	0.19	0.18	0.22
Zn	62	85	51	84	54	71	42	75
Ga	7	7	8	9	12	12	11	13
La	0.74	1.06	0.81	0.10	1.24	0.14	0.26	0.63
Ce	1.14	1.11	1.05	0.39	2.20	0.12	0.52	0.60
Pr	0.16	0.33	0.21	0.12	0.60	0.04	0.15	0.15
Nd	0.65	1.96	1.09	0.98	3.91	0.26	1.09	0.85
Sm	0.14	0.75	0.37	0.60	1.62	0.12	0.58	0.32
Eu	0.13	0.32	0.18	0.28	0.48	0.21	0.37	0.27
Gd	0.16	1.03	0.56	1.04	2.47	0.21	0.96	0.51
Tb	0.03	0.18	0.10	0.20	0.42	0.04	0.17	0.09
Dy	0.17	1.19	0.70	1.46	2.93	0.29	1.24	0.64
Ho	0.04	0.26	0.16	0.34	0.66	0.06	0.28	0.14
Er	0.10	0.72	0.48	0.99	1.86	0.19	0.80	0.42
Tm	0.02	0.11	0.08	0.16	0.28	0.03	0.12	0.06
Yb	0.11	0.68	0.52	1.06	1.80	0.20	0.80	0.43
Lu	0.02	0.10	0.09	0.17	0.27	0.03	0.12	0.07
Y	1.09	7.22	4.67	9.25	18.65	1.79	7.65	4.00
Hf	0.04	0.35	0.23	0.32	0.98	0.04	0.27	0.15
Cs	0.01	0.00	0.00	0.00	0.01	0.00	0.00	0.00
Pb	n.d.	n.d.	n.d.	0.71	1.16	n.d.	n.d.	n.d.
Th	0.03	0.00	0.01	0.01	0.00	0.00	0.00	0.00
U	0.01	0.02	0.00	0.01	0.15	0.00	0.00	0.00

*Pyroxenite-dominated band taken from a corundum-bearing granulite, *KNt02,* of which each compositional band is thick enough to be separated out for analysis and modally equivalent to websterite.

n.d. = not detected

Table 3.3 (cont.)

	Granulites							
	Banded	Banded	Banded	Pl-rich band*	Foliated	Foliated	Foliated	Crn-barren
ppm:	*NG 13*	*NG 20*	*KKa03*	*KNt 02-1**	*OK 02*	*NG 04*	*OK 03*	*KMb 01*
Rb	0.31	1.28	1.10	0.41	0.68	0.66	1.62	0.71
Ba	50	1181	239	104	93	447	184	167
Sr	104	215	329	285	638	563	654	334
V	42	61	13	153	58	18	16	26
Cr	195	168	142	661	350	153	54	50
Ni	649	397	284	403	271	336	200	48
Zr	0.90	1.96	2.58	0.59	0.58	2.26	7.28	0.94
Sc	4	10	3	7	10	2	3	5
Cu	2	2	5	1	0	3	2	5
Nb	0.19	0.17	1.42	0.23	0.21	0.28	1.76	0.48
Zn	58	49	32	100	28	38	24	n.d
Ga	12	12	14	20	13	16	16	21
La	1.91	1.16	0.64	0.34	0.10	0.57	2.56	0.46
Ce	2.77	0.76	0.52	0.40	0.13	0.88	3.97	0.58
Pr	0.30	0.23	0.13	0.09	0.02	0.13	0.53	0.07
Nd	1.07	1.12	0.52	0.39	0.08	0.64	2.04	0.27
Sm	0.24	0.34	0.11	0.08	0.03	0.16	0.36	0.06
Eu	0.22	0.47	0.24	0.13	0.28	0.74	0.49	0.51
Gd	0.31	0.49	0.11	0.09	0.05	0.16	0.30	0.07
Tb	0.05	0.08	0.02	0.01	0.01	0.02	0.04	0.01
Dy	0.36	0.55	0.08	0.08	0.07	0.14	0.17	0.07
Ho	0.08	0.12	0.02	0.02	0.02	0.03	0.03	0.01
Er	0.23	0.34	0.04	0.06	0.06	0.08	0.07	0.04
Tm	0.04	0.05	0.01	0.01	0.01	0.01	0.01	0.01
Yb	0.25	0.33	0.03	0.06	0.07	0.08	0.04	0.04
Lu	0.04	0.05	0.01	0.01	0.01	0.01	0.01	0.01
Y	2.25	3.51	0.66	0.62	0.52	0.85	0.94	0.41
Hf	0.07	0.14	0.05	0.01	0.01	0.06	0.15	0.03
Ta	0.95	1.35	1.86	1.42	1.33	0.46	1.27	0.42
Cs	0.01	0.01	0.01	0.004	0.01	0.00	0.02	0.01
Pb	n.d.	n.d.	1.19	n.d.	n.d.	n.d.	0.11	0.42
Th	0.06	0.00	0.06	0.00	0.01	0.03	0.19	0.01
U	0.02	0.00	0.02	0.02	0.00	0.01	0.06	0.00

*Separated plagioclase-dominated band taken from a corundum-bearing granulite, *KNt02*.
n.d. = not detected.

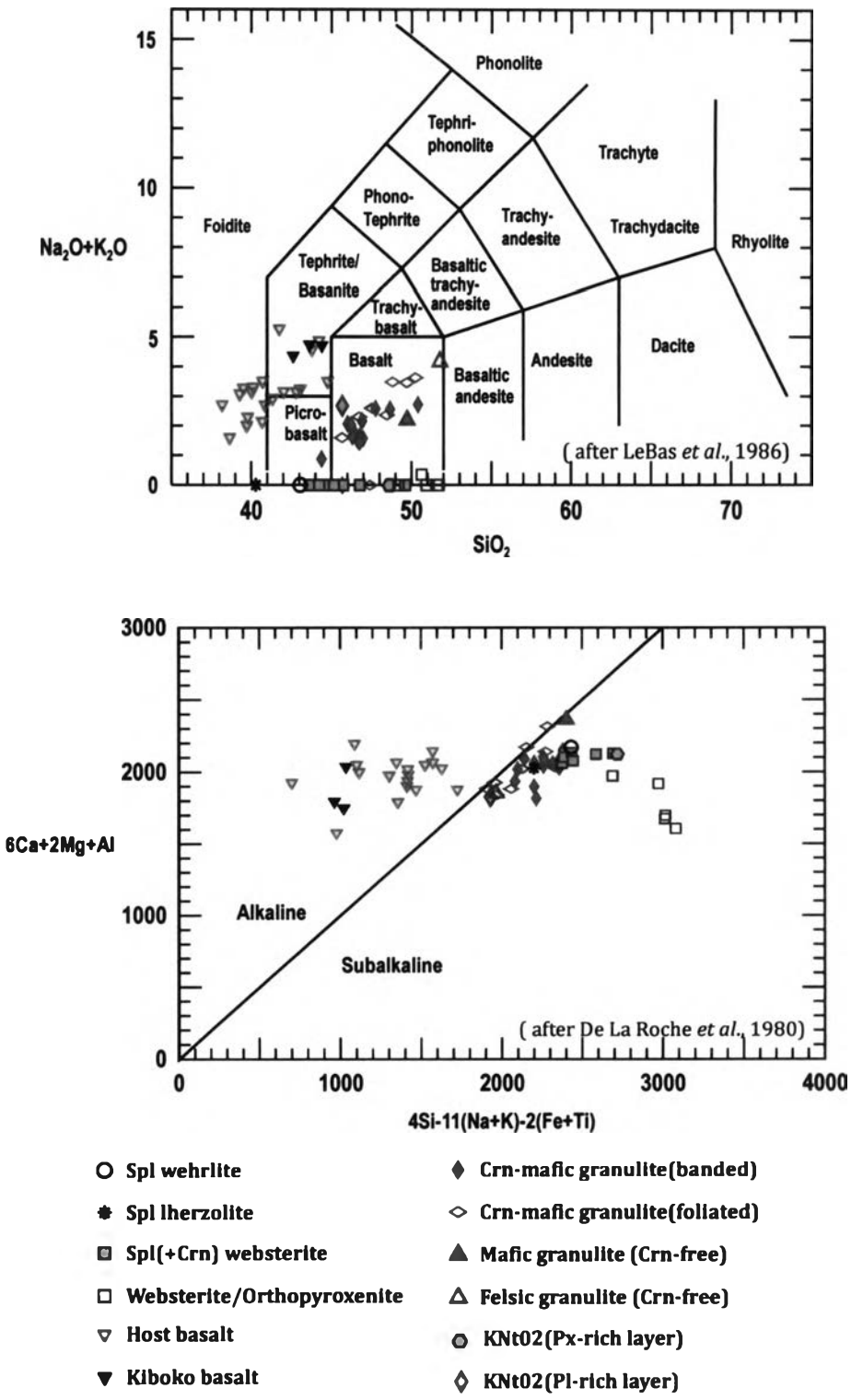

Figure 3.5 ***a*) LeBas *et al.* cassification diagrams for xenoliths from the study sites around the Nguu Hills and Ngulai Hills in comparison to their basaltic hosts. *b*) The alkaline/sub-alkaline subdivision diagram according to De LeRoche *et al.* (1980).**

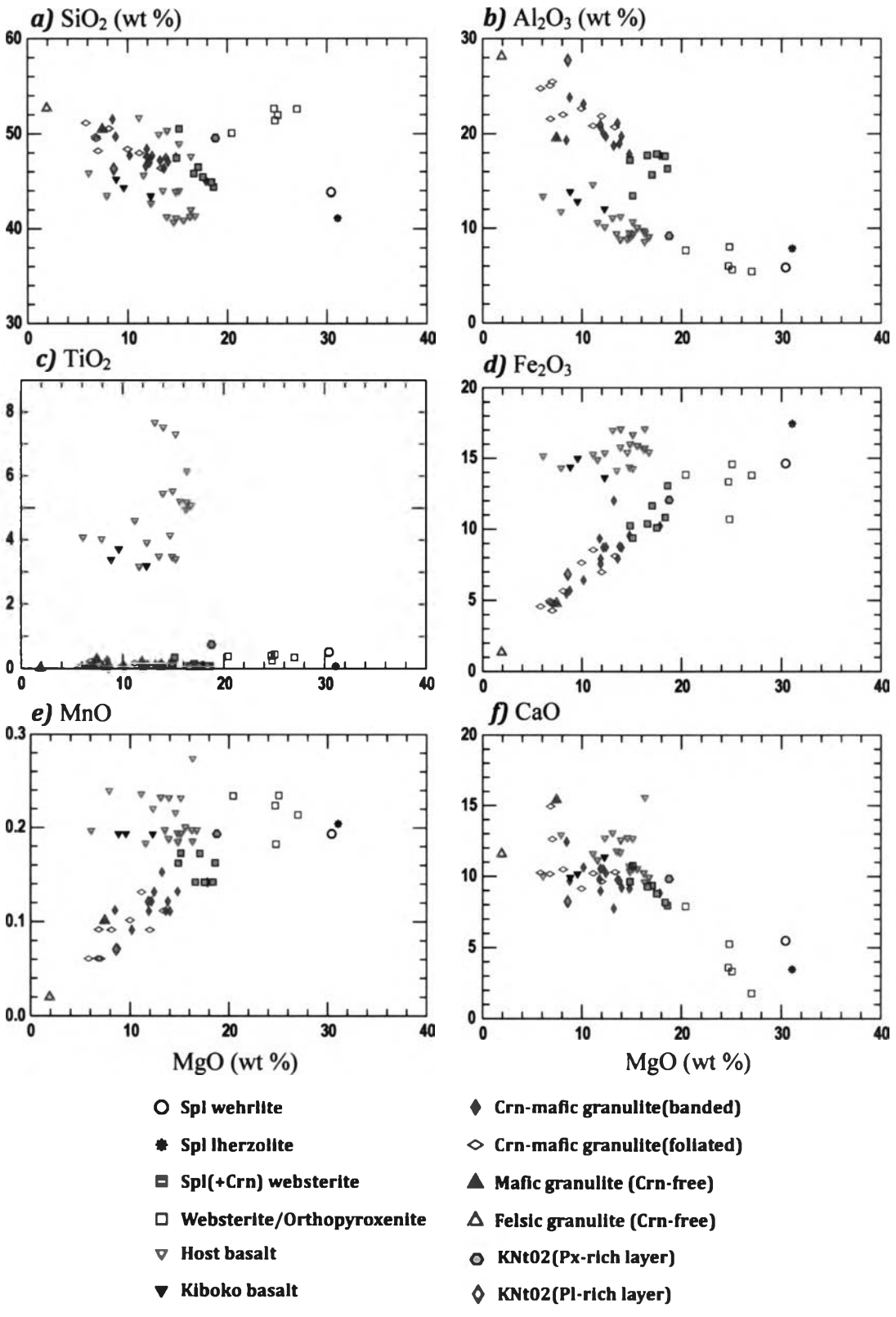

Figure 3.6 MgO variation diagrams for selected major oxides in the studied xenoliths.

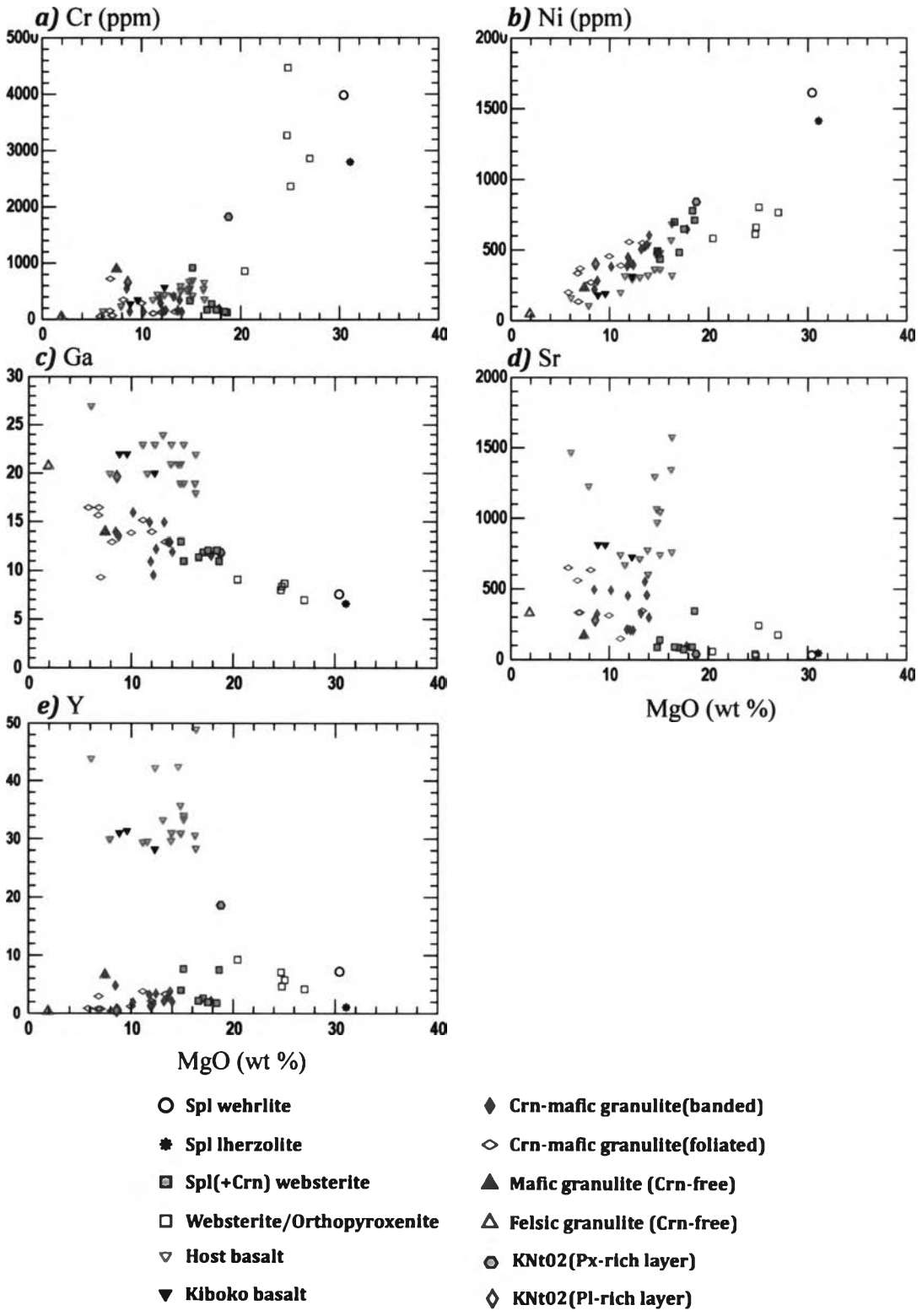

Figure 3.7 MgO variation diagrams for selected trace elements in the studied xenoliths.

ppm as well as Ni form ~1,400 to 1,600 ppm. The *Ng07* also contains high Ba contents of 370 ppm while only 13 ppm for the *Ng18*. Both lithological and chemical, these specimens show the most primitive natures among the whole set of xenoliths.

The pyroxenites have SiO_2 between 43.6 and 51.7 wt %, MgO from 14.7 to 26.5 wt %, $Fe_2O_3^t$ from 9.4 to 13.9 wt % and Al_2O_3 from 5.3 to 17.6 wt %, with An contents in a range of 76–87, slightly lower than the peridotite.). Mg# values are from 0.76 to 0.83. For the spinel-bearing websterite samples, e.g. *Ng23, Ng25* and *Ng 27*, total feldspar normative contents are much higher (40-51 wt % norm) than those of the spinel free ones, e.g. *Ng12* and *Ng29* (~23 wt % norm). Cr and Ni contents are also overall high but quite vary from sample to sample from 136 to 4,464 and 436 to 779 ppm, respectively. The *Ng27* which contains 1.4 wt % norm of corundum has the highest Ni but the lowest Cr contents of the group.

The granulites have SiO_2 between 44.4 and 51.8 wt %, MgO from 1.9 to 13.9 wt %, $Fe_2O_3^t$ from 1.4 to 12.1 wt % and Al_2O_3 from 17.7 to 27.7 wt %, with a wider An range (61 to 85). Mg# values are from 0.73 to 0.84. Obviously, the An contents of the composite banded granulites, e.g. *KNt02*, are much higher in the pyroxene-rich zone (~ 83) than in the plagioclase-rich zone (~ 65). The mg# values are of the same manner, ~84 in the pyroxene-rich and ~73 in the plagioclase-rich band. Several samples, including *OK03, Ng13, Ng04, KKa03* and *KNt02* (Pl-rich zone) have corundum normative, 0.13-8.21 wt % norm. One corundum-barren sample, *KMb01*, has corundum normative of 1.83 wt % as well.

The major oxides plots using MgO as a differentiation index seem to be suitable for this suite of samples as it distinguishes these specimens into groups which are well corresponding to their petrographic appearances. In general, major oxide values of all the xenolith samples continuously align in trends with increasing MgO contents, either with negative or positive slope (Figures 3.6a-f). SiO_2 has a slightly negative trend with increasing MgO, expept those of spinel-free pyroxenites which are displaced from the trend. Al_2O_3, CaO, NaO and total alkali clearly exhibit systematic inverse relationship with MgO. $Fe_2O_3^t$, FeO, MnO, and TiO_2, on the other hands, broadly show positive relationship with MgO.

Although the suite of xenoliths has very low concentration of most incompatible trace elements, several trace elements also behave in correspondent to the major oxides (Figures 3.7a-e). Ga and Sr systematically decrease with increasing MgO as the patterns of Al_2O_3, CaO, NaO and total alkali. On the contrary,

Cr, Ni and Y behave a positive relationship in the same manner with $Fe_2O_3^t$, FeO, MnO, and TiO_2.

Based on pyrolite mantle-normalized multi-element diagrams (McDonough and Sun, 1995), the patterns are generally comparable among samples (Figures 3.8a-f). The normalized incompatible element patterns of the xenoliths suite are clearly different from those of those basts. K depletion patterns do not observed among the xenolith samples. However, depletion patterns of Zr and Nb are obvious instead. Positive Ba and Sr anormalies occur for the majority of the xenoliths, except for fews spinel-free pyroxenites. Acecentuated Eu anorlies are observed in all the granulites and the spinel-bearing websterite as well as the spinel lherzolite, *Ng07*. Unusual positive spikes of Ta are observed in every sample; this, however, might reflect contamination from using a tungstencarbide mill.

The chondrite-normalzied REE patterns (Sun and McDonough, 1989) (Figures 3.9a-f) display a rather flat pattern in most specimens. Positive Eu anomalies are acecentuated in granulites, spl (±crn) websterites and spl lherzolite indicating plagioclase accumulation in the rocks. The REE patterns of the spl(±crn) websterites are indifferent from those of most crn-bearing granulites showing slight enrichment in HREE. Those of the spl-free websterite and spl wehrlite share the pattern similarity of slight HREE enrichment, but without positive Eu anomalies. The spl lherzolite, crn-barren granulite and some crn-bearing granulites, on the other hand, exhibit a slight fractionation of LREE over HREE.

In conclusion, the corundum normative observed in several samples suggested that the xenoliths from the study area bare an Al-rich signature. the whole-rock chemistries show that the abundances of several trace elements are very low for all specimens analyzed including Rb, Zr, Cu, Nb, Th, U, Pb, and most of REE. However, some elements such as Ni and Cr are very high in concentration in most ultramafic specimens. The continuous major oxide and trace element trends of this xenoliths suite, which are similar to normal magma differentiation trends, suggest a close magmatic relationship among all xenoliths. However, several patterns of major oxides and trace elements plotted against MgO clearly indicate that this xenoliths suite is unlikely to share the same parental source with the host basalts. In addition, the mantle-normalized patterns which do not resemble to the host basalts and OIB support this interpretation and further imply that the origin of igneous protholiths were rather not related to a mantle plume activities. The slightly

different REE patterns among groups of the xenoliths possibly reflect either a variation in cumulus nature or heterogeneity of a parental source material.

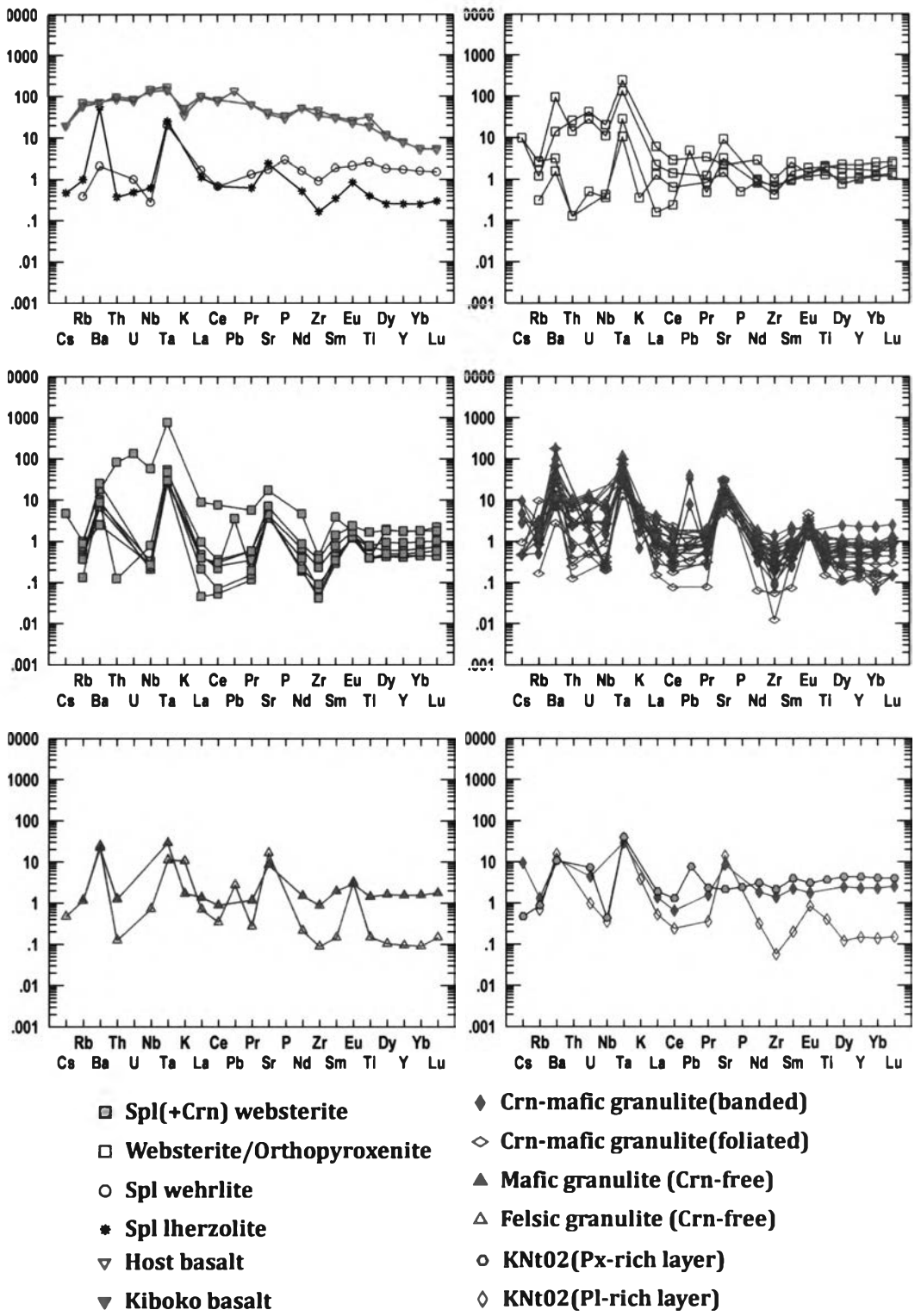

Figure 3.8 Pyrolite mantle normalized patterns of the studied xenoliths compared with representative basalts.. Normalization values are from McDonough and Sun (1995).

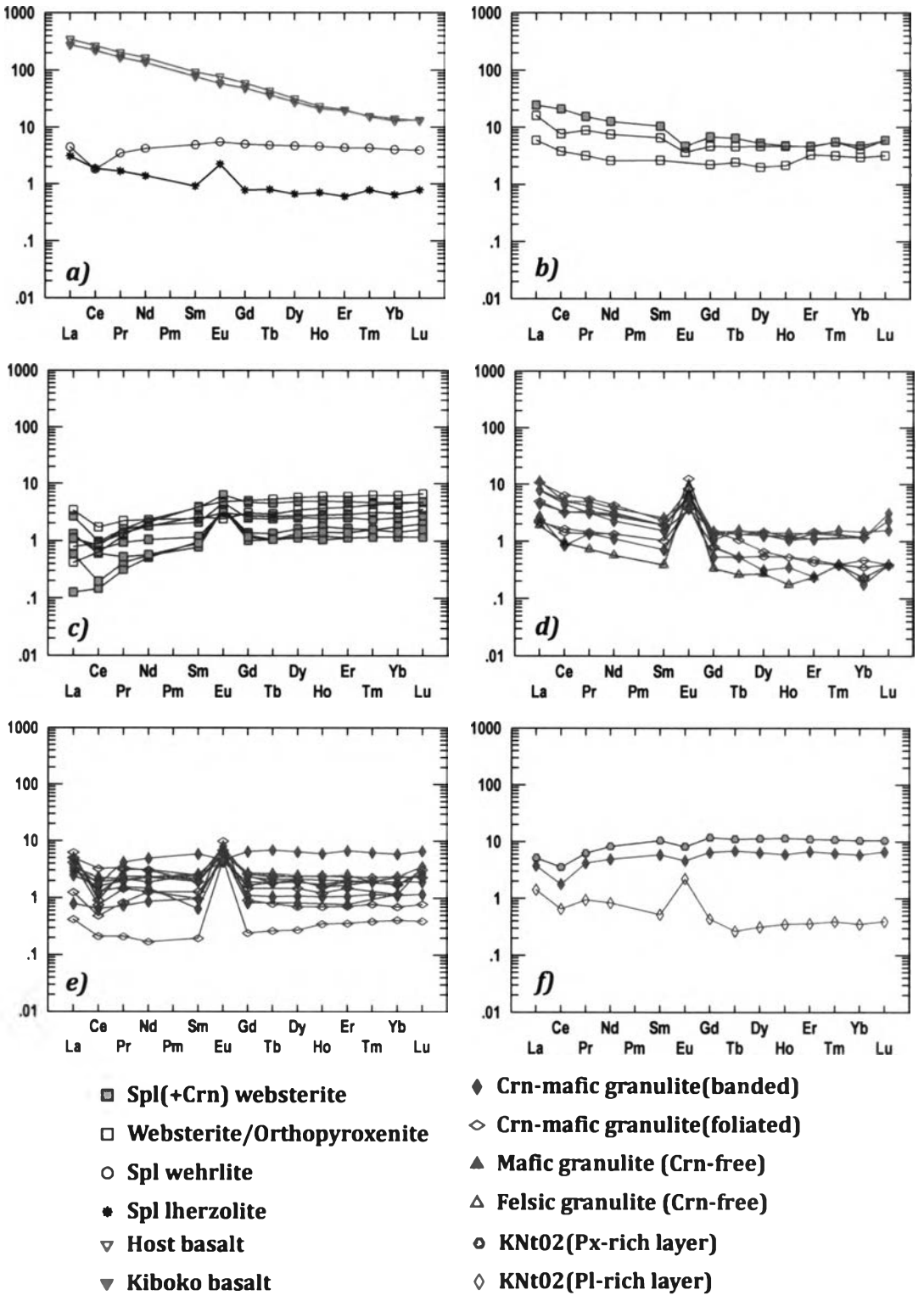

Figure 3.9 Chondrite normalized REE patterns of the studied xenoliths compared with representative basalts. Normalization values are from Sun and McDonough (1989).

3.3 Mineral Chemistry of Xenoliths

In principle, mineral chemistry yields information that may lead to more understading the nature and origins of xenoliths in the host basalts obtained from the study area. As mentioned afore, several types of minerals, e.g. olivine, orthopyroxene, clinopyroxene, garnet, spinel, plagioclase, corundum and kyanite, are found in more than one type of rocks. Some show mutual equilibrium relations among surrounding phase, but some are not. These mineral phases were, therefore analyzed for comparative purposes. As EPMA cannot differentiate between Fe^{2+} and Fe^{3+}, Fe^{3+} contents in iron-bearing minerals that contain various Fe^{2+}/ Fe^{3+}ratios, e.g. pyroxene, garnet and spinel, are estimated by using the method of Droop (1987). The acceptable analyses are listed in Appendix, and selected representative analyses of each phase are presented, described and discussed in the following sections.

3.3.1 Olivine

Olivine occurs only in ultramafic xenoliths of peridotite group (group 1). Chemical analyses of olivine (Table 3.4) have been recalculated to cation formulae on the basis of 4 oxygens, from which the molecular proportions of Mg, Fe, and Mn end-menbers have been obtained.

Olivines in Peridotitic Xenoliths have quite a narrow range of chemical composition. It is almost indifferent between those in the spinel lherzolite and in the spinel wehrltie. However, the olivines in the wehrlite are 2-3% higher in forsterite component.

In spinel lherzolite, the olivines approximately contains 38-40% SiO_2, 41-43% MgO, 18-19% FeO, 0.1-0.2% MnO, 0.2-1.2% NiO and traces of Cr_2O_3 and CaO. Corresponding end-member percentages are 79-81Mg (forsterite; fo) and 19-21Fe (fayalite; fa). However, in the area where the olivines come in contact with kelyphitic garnet, some oxides are subjected to certain degree of modification as a consequence of olivine-garnet interaction, e.g. MgO can be down to about 35% whereas FeO and Al_2O_3 can be raised up to 27% and 9%, respectively.

In spinel wehrlite, the olivines approximately contain 37-40% SiO_2, 44-45% MgO, 15-16% FeO, 0.1-0.2% MnO, 0.3-0.5% NiO, and traces of Cr_2O_3 and CaO.

Table 3.4. Representative EPMA of olivine

Type	Spl Lherzolite								Spl Wehrlite			
Sample No.	Ng07								Ng18			
	ol277	ol281	ol17	ol18	ol23	ol24	ol27	ol27	ol1	ol2	ol3	ol4
SiO2	39.68	39.65	39.65	39.6	39.68	39.67	39.62	39.62	39.6	39.7	39.65	39.65
TiO2	0.00	0.00	0.00	0.01	0.01	0.00	0.02	0.02	0.00	0.00	0.00	0.00
Al2O3	0.00	0.00	0.01	0.01	0.03	0.03	0.03	0.03	0.02	0.00	0.00	0.01
Cr2O3	0.00	0.02	0.01	0.01	0.02	0.00	0.00	0.00	0.04	0.00	0.02	0.01
FeO	15.61	15.66	15.85	15.85	15.66	15.47	15.55	15.55	15.86	15.61	15.66	15.85
MnO	0.08	0.10	0.08	0.12	0.15	0.15	0.15	0.15	0.16	0.10	0.10	0.08
MgO	44.15	44.05	43.91	43.8	44.03	44.14	44.12	44.12	43.9	44.2	44.05	43.91
NiO	0.37	0.42	0.49	0.44	0.34	0.38	0.42	0.42	0.39	0.35	0.42	0.49
ZnO	0.07	0.07	0.00	0.13	0.00	0.14	0.05	0.05	0.00	0.03	0.07	0.00
CaO	0.00	0.00	0.03	0.01	0.00	0.03	0.02	0.02	0.01	0.00	0.00	0.03
Total	99.96	99.97	100.03	99.98	99.92	100.01	99.98	99.98	99.98	99.99	99.97	100.03
Formula 4(O)												
Si	1.000	1.000	1.000	1.000	1.001	1.000	0.999	0.999	1.000	1.000	1.000	1.000
Ti	0.000	0.000	0.000	0.000	0.000	0.000	0.000	0.000	0.000	0.000	0.000	0.000
Al	0.000	0.000	0.000	0.000	0.001	0.001	0.001	0.001	0.001	0.000	0.000	0.000
Cr	0.000	0.000	0.000	0.000	0.000	0.000	0.000	0.000	0.001	0.000	0.000	0.000
Fe	0.329	0.330	0.334	0.335	0.330	0.326	0.328	0.328	0.335	0.329	0.330	0.334
Mn	0.002	0.002	0.002	0.003	0.003	0.003	0.003	0.003	0.003	0.002	0.002	0.002
Mg	1.659	1.657	1.651	1.649	1.655	1.658	1.659	1.659	1.652	1.660	1.657	1.651
Ni	0.008	0.009	0.010	0.009	0.007	0.008	0.009	0.009	0.008	0.007	0.009	0.010
Zn	0.001	0.001	0.000	0.002	0.000	0.003	0.001	0.001	0.000	0.001	0.001	0.000
Ca	0.000	0.000	0.001	0.000	0.000	0.001	0.001	0.001	0.000	0.000	0.000	0.001
Total	2.999	2.999	2.998	2.998	2.997	3.000	3.001	3.001	3.000	2.999	2.999	2.998
Atomic %												
Mg	83.4	83.3	83.1	83.0	83.2	83.4	83.4	83.4	83.0	83.4	83.3	83.1
Fe	16.5	16.6	16.8	16.9	16.6	16.4	16.5	16.5	16.8	16.5	16.6	16.8
Mn	0.1	0.1	0.1	0.2	0.2	0.2	0.2	0.2	0.2	0.1	0.1	0.1

corresponding end-member percentages are 83-84Mg (forsterite; fo) and 16-17Fe (fayalite; fa).

Similarities in composition of olivines in both samples suggest that they are likely generated from the same source, but may not be derived from an ultramafic source. This is due to the poorer forsterite contents when compared to those in other mafic-ultramafic xenoliths from elsewhere, such as Group I San Carlos ultramafic xenoliths from U.S.A. (Frey and Prinz, 1978), xenoliths from eastern China (Fan and Hooper, 1989), southern China (Qi *et al.*, 1995), Society Islands of Tahiti (Qi *et al.*, 1994) and Thailand (Promprated *et al.*, 1999; Sutthirat, 2001), lherzolite from northern Italy (Obata and Morten, 1987), garnet-bearing ultramafic rock from Bohemian Massif (Schmädicke and Evans, 1997) and some ultramafic rock units of ophiolite suites from inner Mongolia, China (Robinson *et al.*, 1999), which generally fall in the range of 85-91% fo. However, the forsterite contents are comparable to some fo-poorer (down to about 78% fo) ultramafic xenoliths from Taiti. Qi *et al.* (1994) interpreted them as a part of cumulates of basaltic magma. This, therefore, could presumably be the case for Ng 07. Positive Eu anomaly pattern from its whole-rock analysis as also supported this interpretation.

3.3.2 Orthopyroxene

Orthopyroxenes are another major phase found in ultramafic xenoliths, particularly pyroxenite group (group 2). Chemical analyses of orthopyroxenes have been recalculated to cation formulae on the basis of 6 oxygens, with Fe^{3+} estimation (Table 3.5). Normalized atomic percentages of Mg, Fe^{2+}, and Ca are calculated for plotting on the pyroxene quadrilateral (Figure 3.8). Apart from unaffected core area, the analyses are also undertaken in some reaction areas, e.g. spongy edges, sieved textures and symplectic/reaction coronas. Unfortunately, most of the results from these areas are not usable. Therefore, they will be less considered in the study.

Orthopyroxene in Peridotitic Xenoliths

In spinel lherzolite, the orthopyroxenes can be separated into 2 group based on their CaO contents: (1) primary (higher-Ca) phase and (2) secondary (lower-Ca) phase. The primary phase consists of 52-55% SiO_2, 25-30% MgO, 11-16% FeO^t (8-13% FeO, 2.5-3.6% Fe_2O_3), 1.8-2.9% Al_2O_3, 1.7-2.5% CaO, 0.1-0.5%

MnO, 0.1-0.5% Cr_2O_3, and traces of TiO_2, NiO and Na_2O. Corresponding Mg# values are of 74-83% and normalized atomic proportions of about 73-85% Mg, 12-22% Fe^{2+}, and 3-5% Ca.

The secondary phase approximately contains 54-56% SiO_2, 30-31% MgO, 11% FeO^t (7-11% FeO, ≤4.5% Fe_2O_3), 1.8-2.4% Al_2O_3, ≤1% CaO, ≤0.7% NiO and traces of Cr_2O_3, TiO_2, MnO and Na_2O. Corresponding Mg# values are of 83-84% and normalized atomic proportions of about 82-88% Mg, 11-16% Fe^{2+}, and 1-2% Ca.

Table 3.5 Representative EPMA of orthopyroxene in the peridotites.

Type	Spl Lherzolite			Spl Wehrlite				
Sample No.	Ng07			Ng18				
	opx18	opx20	opx304	opx4	opx244	opx243	opx262	opx245
SiO_2	54.15	54.74	52.28	50.34	51.59	50.24	48.17	46.78
TiO_2	0.15	0.16	0.04	0.17	0.03	0.00	0.01	0.00
Al_2O_3	1.81	1.95	2.93	6.64	7.01	8.17	10.80	14.12
Cr_2O_3	0.17	0.15	0.50	0.51	0.47	0.45	0.57	0.68
Fe_2O_3	3.59	2.52	2.63	2.19	0.00	0.29	1.56	0.00
FeO	7.70	8.39	13.41	13.26	14.46	15.14	12.88	15.00
MnO	0.13	0.20	0.51	0.59	0.49	0.39	0.37	0.44
MgO	30.17	30.03	25.40	24.72	24.21	23.53	23.21	20.63
NiO	0.00	0.00	0.03	0.04	0.03	0.00	0.00	0.00
CaO	1.68	1.93	2.50	1.82	1.80	1.93	2.27	2.67
Na_2O	0.19	0.21	0.03	0.01	0.03	0.02	0.01	0.03
K_2O	0.00	0.00	0.00	0.00	0.00	0.00	0.01	0.02
Total	99.75	100.27	100.26	100.30	100.11	100.14	99.85	100.36
Formula 6(O)								
Si	1.914	1.927	1.894	1.817	1.862	1.816	1.741	1.692
Ti	0.004	0.004	0.001	0.005	0.001	0.000	0.000	0.000
Al^{iv}	0.070	0.062	0.094	0.173	0.144	0.182	0.252	0.308
Al^{vi}	0.005	0.019	0.031	0.110	0.154	0.166	0.208	0.294
Cr	0.005	0.004	0.014	0.014	0.013	0.013	0.016	0.019
Fe^{3+}	0.096	0.067	0.072	0.060	0.000	0.008	0.042	0.000
Fe^{2+}	0.228	0.247	0.406	0.400	0.436	0.458	0.389	0.454
Mn	0.004	0.006	0.016	0.018	0.015	0.012	0.011	0.013
Mg	1.589	1.576	1.372	1.331	1.302	1.268	1.251	1.113
Ni	0.000	0.000	0.001	0.001	0.001	0.000	0.000	0.000
Ca	0.064	0.073	0.097	0.070	0.070	0.075	0.088	0.103
Na	0.013	0.014	0.002	0.001	0.002	0.002	0.001	0.002
K	0.000	0.000	0.000	0.000	0.000	0.000	0.000	0.001
Total	3.991	3.999	4.000	4.000	4.000	3.999	4.000	4.000
Atomic %								
Mg	0.85	0.83	0.73	0.22	0.24	0.25	0.72	0.27
Fe	0.12	0.13	0.22	0.04	0.04	0.04	0.23	0.06
Ca	0.03	0.04	0.05	73.57	74.26	72.65	0.05	70.43
Mg#	82.90	83.12	73.53	1.817	1.862	1.816	73.84	1.692

Table 3.5 (cont.) Representative EPMA of orthopyroxene in the pyroxenites.

Type	Orthopyroxenite			Spl-free websterite				
Sample No.	Ng33			Ng12		Ng34		
	opx48	opx45	opx55	opx74	opx158	opx117	opx120	opx125
SiO_2	49.48	47.62	45.79	54.52	55.01	55.37	55.60	55.24
TiO_2	0.03	0.01	0.01	0.00	0.06	0.02	0.02	0.02
Al_2O_3	11.21	14.30	17.01	1.94	2.61	2.17	2.52	2.15
Cr_2O_3	1.04	1.09	1.34	0.31	0.09	0.36	0.42	0.41
Fe_2O_3	1.55	1.35	1.45	1.38	0.00	0.00	0.00	0.31
FeO	4.95	5.35	5.14	9.13	10.15	12.28	11.27	11.77
MnO	0.34	0.38	0.26	0.10	0.09	0.06	0.17	0.18
MgO	29.46	27.90	26.69	30.56	30.27	29.45	27.94	29.45
NiO	0.00	0.00	0.01	0.15	0.00	0.10	0.06	0.10
CaO	1.07	1.11	1.38	0.70	0.60	0.51	1.86	0.73
Na_2O	0.00	0.01	0.00	0.10	0.03	0.10	0.38	0.13
K_2O	0.01	0.00	0.01	0.00	0.00	0.01	0.00	0.00
Total	99.12	99.11	99.09	98.88	98.91	100.42	100.23	100.49
Formula 6(O)								
Si	1.777	1.716	1.655	1.940	1.954	1.955	1.969	1.949
Ti	0.001	0.000	0.000	0.000	0.002	0.001	0.000	0.001
Al^{iv}	0.230	0.292	0.352	0.054	0.050	0.046	0.036	0.049
Al^{vi}	0.228	0.294	0.345	0.027	0.060	0.045	0.069	0.040
Cr	0.028	0.030	0.037	0.009	0.003	0.010	0.012	0.011
Fe^{3+}	0.000	0.000	0.000	0.037	0.000	0.000	0.000	0.008
Fe^{2+}	0.184	0.191	0.187	0.272	0.302	0.362	0.334	0.347
Mn	0.010	0.011	0.008	0.003	0.003	0.002	0.005	0.005
Mg	1.502	1.424	1.364	1.621	1.603	1.550	1.475	1.549
Ni	0.000	0.000	0.000	0.004	0.000	0.003	0.002	0.003
Ca	0.040	0.041	0.051	0.027	0.023	0.019	0.071	0.028
Na	0.000	0.001	0.000	0.007	0.002	0.007	0.026	0.009
K	0.000	0.000	0.000	0.000	0.000	0.000	0.000	0.000
Total	4.000	4.000	4.000	4.000	4.000	4.000	3.999	4.000
Atomic %								
Mg	0.87	0.86	0.85	0.84	0.83	0.80	0.78	0.81
Fe	0.11	0.12	0.12	0.14	0.16	0.19	0.18	0.18
Ca	0.02	0.02	0.03	0.01	0.01	0.01	0.04	0.01
Mg#	88.57	87.58	87.49	83.88	84.04	80.98	81.33	81.11

In spinel wehrlite, the orthopyroxenes can be separated into 2 group based on their CaO contents: (1) primary (higher-Ca) phase and (2) secondary (lower-Ca) phase. The primary phase is composed of 46-52% SiO_2, 18-25% MgO, 14-22% FeO^t (12-22% FeO, <3% Fe_2O_3), 7-14% Al_2O_3, 1.7-2.5% CaO, 0.1-0.5% MnO, 0.1-0.5% Cr_2O_3,and traces of TiO_2, NiO and Na_2O. Corresponding Mg# values are of 58-74% and normalized atomic proportions of about 58-74% Mg, 21-40% Fe^{2+}, and 2-6% Ca. The secondary phase approximately contains 55-56% SiO_2, 31-32% MgO, 10% FeO^t (8-10% FeO, ≤2.6% Fe_2O_3), 2% Al_2O_3, 0.3-0.4% CaO, 0.2-0.3% Cr_2O_3, ≤0.2% NiO and

traces of TiO_2, MnO and Na_2O. Corresponding $Mg^{\#}$ values are of 84-85% and normalized atomic proportions of 84-88% Mg, 12-15% Fe^{2+}, and $\leq$1% Ca.

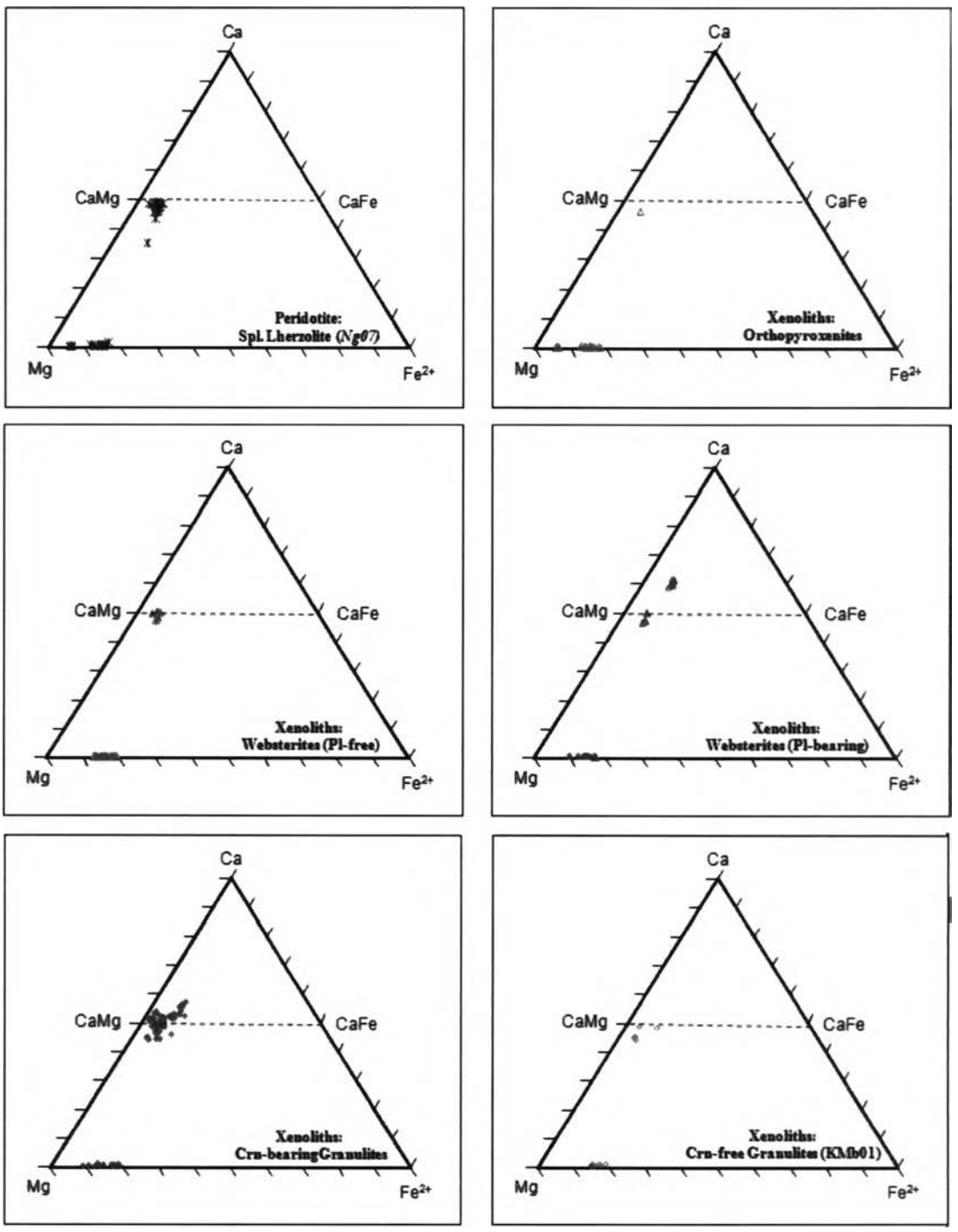

Figure 3.10 Pyroxene plots of Fe^{2+}-Ca-Mg atomic proportions of orthopyroxenes and clinopyroxenes in peridotite, pyroxenite and granulite xenoliths.

Orthopyroxene in Pyroxenitic Xenoliths

In orthopyroxenite, the orthopyroxenes can be separated into 2 groups based on their CaO contents: (1) primary (higher-Ca) phase and (2) secondary (lower-Ca) phase. The primary phase consists of 46-50% SiO_2, 26-29% MgO, 6% FeO^t (5% FeO, ≤1.5% Fe_2O_3), 11-17% Al_2O_3, <1.4% CaO, <1.5 % Cr_2O_3, ≤0.1% NiO and traces of TiO_2, MnO and Na_2O. Corresponding Mg# values are of 88-89% and normalized atomic proportions of 85-87% Mg, 11-12% Fe^{2+} and 2-3% Ca.

The secondary phase approximately contains 54-58% SiO_2, 30-36% MgO, 4-13% FeO^t (4-11% FeO, ≤4% Fe_2O_3), 2-3% Al_2O_3, <0.5% CaO, <0.6% Cr_2O_3, ≤0.1% NiO and traces of TiO_2, MnO and Na_2O. Corresponding Mg# values are of 81-94% andnormalized atomic proportions of 82-94% Mg, 6-17% Fe^{2+}, and ≤1% Ca. Comparatively, the orthopyroxenite xenolith collected from Nguu Hills (Ng33) has higher SiO_2 content (57-58%) and much higher Mg# value (93-94%) than those from Ngulai Hills (KNt03: 54-55% SiO_2, 81-82% Mg#), but lower in FeO (Ng33:4-4.%; KNt03:9-11%) and Fe2O3 (Ng33:trace; KNt03:1-4%) contents.

In websterite, the orthopyroxenes can be separated into 2 groups based on their CaO contents which are (1) primary (higher-Ca) phase and (2) secondary (lower-Ca) phase. The primary phase consists of 54-56% SiO_2, 28-31% MgO, 10-12% FeO^t (9-12% FeO, ≤1.5% Fe_2O_3), 2-3% Al_2O_3, <2% CaO, <0.5% Na_2O, <0.5 % Cr_2O_3 and traces of TiO_2, MnO and NiO. Corresponding Mg# values are of 81-84% and normalized atomic proportions of 78-84% Mg, 14-19% Fe^{2+} and 1-4% Ca.

The secondary phase approximately contains 54-57% SiO_2, 30-32% MgO, 9-13% FeO^t (8-13% FeO, ≤3% Fe_2O_3), <3% Al_2O_3, <0.5% CaO, <0.5% Cr_2O_3, <0.2% NiO and traces of TiO_2, MnO and Na_2O. Corresponding Mg# values are of 80-86% and normalized atomic proportions of 80-87% Mg, 13-19% Fe^{2+}, and ≤1% Ca.

3.3.3 Clinopyroxene

Clinopyroxenes are another major phase of all xenoliths types, except for the orthopyroxenitic variety of group 2. Chemical analyses of clinopyroxene have been recalculated in the same manner with orthopyroxene and presented in Table 3.6. Normalized atomic percentages of Mg, Fe^{2+}, and Ca are calculated for plotting on the pyroxene quadrilateral (Figure 3.10). The analyses were carried out on every generation of clinopyroxene observed, but main focus is on a large primary phase.

Clinopyroxene in Peridotitic Xenoliths

In spinel lhzolite, the clinopyroxenes can also be separated into 2 groups based on their Al_2O_3 contents which are (1) primary (higher-Al) phase and (2) secondary (lower-Al) phase. The primary phase roughly contains 53-55% SiO_2, 15-20% CaO, 13-17% MgO, 3-5% FeO^t (2-5% FeO, ≤2% Fe_2O_3), 6-8% Al_2O_3, 2-3%Na_2O, ≤0.4% NiO, 0.2-0.4% Cr_2O_3, ≤0.3% TiO_2, and traces of MnO. Corresponding Mg# values are of 85-87% and normalized atomic proportions of about 44-55% Mg, 35-49% Ca and 4-10% Fe^{2+}.

Table 3.6 Representative EPMA of orthopyroxene in the peridotites.

Type	Spl Lherzolite				Spl Wehrlite			
Sample No.	Ng07				Ng18			
	cp35	cp188	cp102	cp126	cp110	cp7	cp16	cp102
SiO_2	52.61	53.79	53.02	53.54	53.69	54.01	53.18	53.02
TiO_2	0.34	0.17	0.59	0.00	0.37	0.34	0.37	0.59
Al_2O_3	7.92	6.86	2.74	6.76	2.83	3.90	3.62	2.74
Cr_2O_3	0.36	0.26	0.68	0.29	0.54	0.60	0.59	0.68
Fe_2O_3	0.00	0.00	1.61	0.00	0.04	0.00	1.02	1.61
FeO	3.60	3.93	3.81	5.40	4.52	4.47	3.54	3.81
MnO	0.03	0.03	0.15	0.06	0.06	0.07	0.06	0.15
MgO	13.27	13.45	14.90	16.78	14.97	15.41	15.33	14.90
NiO	0.00	0.01	0.03	0.02	0.04	0.04	0.06	0.03
CaO	19.14	19.53	21.29	15.00	21.71	19.19	20.32	21.29
Na_2O	2.72	1.77	1.30	1.87	1.16	1.67	1.48	1.30
K_2O	0.02	0.01	0.03	0.00	0.00	0.02	0.02	0.03
Total	100.02	99.80	100.17	99.73	99.97	99.73	99.61	100.17
Formula 6(O)								
Si	1.894	1.957	1.939	1.929	1.962	1.965	1.942	1.939
Ti	0.009	0.005	0.016	0.000	0.010	0.009	0.010	0.016
Al^{iv}	0.100	0.059	0.053	0.075	0.038	0.038	0.053	0.053
Al^{vi}	0.236	0.235	0.065	0.212	0.084	0.130	0.102	0.065
Cr	0.010	0.007	0.020	0.008	0.016	0.017	0.017	0.020
Fe^{3+}	0.000	0.000	0.045	0.000	0.001	0.000	0.028	0.045
Fe^{2+}	0.108	0.120	0.117	0.163	0.138	0.136	0.108	0.117
Mn	0.001	0.001	0.005	0.002	0.002	0.002	0.002	0.005
Mg	0.712	0.729	0.813	0.901	0.815	0.836	0.834	0.813
Ni	0.000	0.000	0.001	0.000	0.001	0.001	0.002	0.001
Ca	0.738	0.761	0.834	0.579	0.850	0.748	0.795	0.834
Na	0.190	0.125	0.092	0.131	0.082	0.118	0.104	0.092
K	0.001	0.000	0.001	0.000	0.000	0.001	0.001	0.001
Total	4.000	4.000	4.000	4.000	4.000	4.000	4.000	4.000
Atomic %								
Mg	0.46	0.45	0.46	0.55	0.45	0.49	0.48	0.46
Fe	0.07	0.07	0.07	0.10	0.08	0.08	0.06	0.07
Ca	0.47	0.47	0.47	0.35	0.47	0.43	0.46	0.47
Mg#	86.69	85.82	83.05	84.55	85.24	85.82	85.80	83.05

Table 3.6 (cont.) Representative EPMA of clinopyroxene in the pyroxenites.

Type	Spl-free websterite						Spl websterite		
Sample No.	Ng12			Ng34			Ng27		
	cp151	cp21	cp154	cp123	cp132	cp137	cpx216	cp29	cpx35
SiO_2	52.76	51.66	54.12	54.93	54.85	54.83	53.81	53.87	54.02
TiO_2	0.25	0.06	0.25	0.09	0.02	0.07	0.04	0.24	0.35
Al_2O_3	7.52	6.95	6.49	6.04	5.93	6.04	7.76	7.38	6.48
Cr_2O_3	0.79	1.14	0.93	0.94	1.27	1.26	0.01	0.00	0.01
Fe_2O_3	0.00	0.45	0.00	0.00	0.00	0.00	0.00	0.00	0.00
FeO	3.22	2.75	3.35	4.25	4.20	4.24	3.64	3.63	3.44
MnO	0.05	0.09	0.06	0.09	0.01	0.04	0.07	0.04	0.00
MgO	12.49	13.06	12.84	12.58	12.67	12.69	12.88	12.71	13.36
NiO	0.05	0.06	0.07	0.00	0.02	0.06	0.05	0.06	0.05
CaO	19.91	20.68	19.08	17.79	18.21	17.71	19.09	19.02	20.01
Na_2O	2.17	1.97	2.56	3.10	3.14	3.06	2.78	2.66	2.44
K_2O	0.02	0.01	0.00	0.00	0.00	0.02	0.00	0.01	0.00
Total	99.25	98.87	99.79	99.80	100.36	100.01	100.14	99.62	100.16
Formula 6(O)									
Si	1.929	1.896	1.965	1.992	1.978	1.986	2.091	2.109	2.112
Ti	0.007	0.002	0.007	0.002	0.001	0.002	0.001	0.007	0.010
Al^{iv}	0.082	0.102	0.046	0.017	0.026	0.023	0.000	0.000	0.000
Al^{vi}	0.242	0.198	0.231	0.241	0.226	0.234	0.355	0.340	0.299
Cr	0.023	0.033	0.027	0.027	0.036	0.036	0.000	0.000	0.000
Fe^{3+}	0.000	0.012	0.000	0.000	0.000	0.000	0.000	0.000	0.000
Fe^{2+}	0.098	0.084	0.102	0.129	0.127	0.128	0.118	0.119	0.113
Mn	0.001	0.003	0.002	0.003	0.000	0.001	0.004	0.002	0.000
Mg	0.681	0.715	0.695	0.680	0.681	0.685	0.424	0.421	0.442
Ni	0.001	0.002	0.002	0.000	0.001	0.002	0.002	0.002	0.001
Ca	0.780	0.813	0.742	0.691	0.704	0.687	0.795	0.797	0.838
Na	0.154	0.140	0.180	0.218	0.219	0.215	0.209	0.202	0.185
K	0.001	0.000	0.000	0.000	0.000	0.001	0.000	0.000	0.000
Total	4.000	4.000	4.000	4.000	4.000	4.000	4.000	4.000	4.000
Atomic %									
Mg	0.44	0.44	0.45	0.45	0.45	0.46	0.32	0.32	0.32
Fe	0.06	0.05	0.07	0.09	0.08	0.09	0.09	0.09	0.08
Ca	0.50	0.50	0.48	0.46	0.47	0.46	0.59	0.60	0.60
Mg#	87.22	87.77	87.03	83.81	84.30	84.09	77.61	77.70	79.72

The secondary phase consists of 53-55% SiO_2, 19-22% CaO, 14-16% MgO, 4% FeO^t (1-4% FeO, <3% Fe_2O_3), 4-5% Al_2O_3, <3% Na_2O, <1 % Cr_2O_3, ≤0.5% NiO and traces of TiO_2 and MnO. Corresponding Mg# values are of 86-88% and normalized atomic proportions of 46-51% Mg, 45-48% Ca and2-7% Fe^{2+}.

In spinel wehrlite, the clinopyroxenes approximately contain 53-54% SiO_2, 19-22% CaO, 15% MgO, 4-5% FeO^t (3-5% FeO, ≤1.6% Fe_2O_3), 3-4% Al_2O_3, 1-2%Na_2O, <1% Cr_2O_3, ≤0.6% TiO_2, and traces of MnO and NiO. Corresponding Mg# values are of 83-86% and normalized atomic proportions of about 45-49% Mg, 43-47% Ca and 6-8% Fe^{2+}.

Clinopyroxene in Pyroxenitic Xenoliths

In orthopyroxenite, the clinopyroxenes approximately contain 51-52% SiO_2, 20-21% CaO, 14-15% MgO, 5-6% FeO^t (3-4% FeO, 2-3% Fe_2O_3), 3-4% Al_2O_3, $\leq$1.5%Na_2O, <0.5% Cr_2O_3, <1% TiO_2, and traces of MnO and NiO. Corresponding $Mg^{\#}$ values are of 82-83% and normalized atomic proportions of about 46-47% Mg, 43-47% Ca and 6-7% Fe^{2+}.

In websterite, the clinopyroxenes can also be separated into 2 groups based on their Al_2O_3 contents which are (1) primary (higher-Al) phase and (2) secondary (lower-Al) phase. The primary phase roughly contains 52-55% SiO_2, 18-21% CaO, 12-14% MgO, 3-5% FeO^t (2-5% FeO, $\leq$2% Fe_2O_3), 6-8% Al_2O_3, 2-3%Na_2O, $\leq$0.1% NiO, <1.3% Cr_2O_3, $\leq$0.3% TiO_2, and traces of MnO. Corresponding $Mg^{\#}$ values are of 83-88% and normalized atomic proportions of about 44-46% Mg, 46-50% Ca and 4-9% Fe^{2+}.

The secondary phase consists of 53-56% SiO_2, 19-22% CaO, 13-15% MgO, 3-4% FeO^t (2-4% FeO, $\leq$1% Fe_2O_3), 3-5% Al_2O_3, <3% Na_2O, <1.5 % Cr_2O_3, $\leq$0.1% NiO and traces of TiO_2 and MnO. Corresponding $Mg^{\#}$ values are of 84-90% and normalized atomic proportions of 45-49% Mg, 45-50% Ca and 4-8% Fe^{2+}.